**Endothelial PHD2 Deficiency Induces Nitrative Stress via Suppression of Caveolin-1 in Pulmonary Arterial Hypertension**

Bin Liu[1,2], Dan Yi[1,2], Jingbo Dai[4,5], Yi Peng[4,5,] Rebecca Vanderpool[3], Maggie M. Zhu[4,5], Zhiyu Dai[1,2†], and You-Yang Zhao[4-8†]

[1]Department of Internal Medicine, [2]Translational Cardiovascular Research Center, College of Medicine-Phoenix, University of Arizona, Phoenix, Arizona, USA;

[3]College of Medicine Division of Cardiovascular Medicine, The Ohio State University, Columbus, Ohio, USA;

[4]Program for Lung and Vascular Biology and [4]Section for Injury Repair and Regeneration Research, Stanley Manne Children's Research Institute, Ann & Robert H. Lurie Children's Hospital of Chicago, Chicago, Illinois, USA;

[5]Departments of Pediatrics, [6]Pharmacology and [7]Medicine, [8]Feinberg Cardiovascular and Renal Research Institute, Northwestern University Feinberg School of Medicine, Chicago, Illinois, USA.

[†]**Correspondence to:** You-Yang Zhao, Ph.D., (youyang.zhao@northwestern.edu), Program for Lung and Vascular Biology, Stanley Manne Children's Research Institute, Ann & Robert H. Lurie Children's Hospital of Chicago, Department of Pediatrics, Northwestern University Feinberg School of Medicine. 225 E Chicago Ave., Box 205. Chicago, IL 60611. Phone: (312) 355-7593.

Or Zhiyu Dai, Ph.D., (zhiyudai@arizona.edu), Department of Internal Medicine, College of Medicine-Phoenix, University of Arizona, 475 N 5th Street, BSPB E512, Phoenix, AZ, 85004. Phone (602)827-2982.

**Running Title: PHD2 deficiency induces nitrative stress in PAH**

**Abstract**

Nitrative stress is a characteristic feature of the pathology of human pulmonary arterial hypertension (PAH). However, the role of nitrative stress in the pathogenesis of obliterative vascular remolding and severe PAH remains largely unclear. Our recent studies identified a novel mouse model (*Egln1*$^{Tie2Cre}$, *Egln1* encoding prolyl hydroxylase 2 [PHD2]) with obliterative vascular remodeling and right heart failure, which provides us an excellent model to study the role of nitrative stress in obliterative vascular remodeling. Here we show that nitrative stress was markedly elevated whereas endothelial Caveolin-1 (Cav1) expression was suppressed in the lungs of *Egln1*$^{Tie2Cre}$ mice. ROS scavenger manganese (III) tetrakis (1-methyl-4-pyridyl) porphyrin pentachloride (MnTmPyP) treatment inhibited obliterative pulmonary vascular remodeling and suppressed severe PAH in *Egln1*$^{Tie2Cre}$ mice. Genetic restoration of endothelial Cav1 expression in *Egln1*$^{Tie2Cre}$ mice normalized nitrative stress, reduced PAH and improved right heart function. These data suggest that suppression of endothelial Cav1 expression secondary to PHD2 deficiency augments nitrative stress, which contributes to obliterative vascular remodeling and severe PAH. Thus, ROS scavenger might have great therapeutic potential for the inhibition of obliterative vascular remodeling and severe PAH.

**Key words:** Endothelial cells, HIF, oxidative stress, nitrative stress, ROS

## Introduction

Pulmonary arterial hypertension (PAH) is a devastating disease characterized by persistent increase of pulmonary vascular resistance and obstructive pulmonary vascular remodeling, which lead to right-sided heart failure and premature death (1–4). Histopathological features of PAH from different etiologies include increased vessel wall thickness, vascular fibrosis, augmented oxidative/nitrative stress, microvascular occlusion and complex plexiform lesions (5–7). Given the molecular mechanisms of obliterative pulmonary vascular remodeling are not fully understood, the current PAH therapies targeting mainly vasoconstriction with little effect on vascular remodeling are not effective in curing the disease and promoting survival (8, 9).

There are accumulating evidence of oxidative stress in the lungs of IPAH patients. Xanthine oxidase activity involved in the generation of superoxide anions and peroxynitrite are markedly increased in IPAH lungs(10), and they contribute to chronic hypoxia-induced PH(11). NADPH oxidases including Nox1, 2, and 4, which also produce high levels of ROS, have been demonstrated to be involved in the development of PAH. [ref] 8-Hydroxyguanosine staining is prominent in endothelial cells (ECs) within the plexiform lesions of IPAH patients(12). 8-Hydroxyguanosine is a biomarker of oxidative damage caused by reaction of superoxide with guanine. In contrary, antioxidants such as manganese superoxide dismutase (MnSOD, a key mitochondrial antioxidant enzyme coded by the SOD2 gene) activity was lower in IPAH lungs (12, 13). Excessive production of nitric oxide and superoxide leads to formation of the damaging reactive oxygen species peroxynitrite(14, 15). Elevated levels of

peroxynitrite (i.e., nitrative stress) are detrimental, which induce cell damage and death of pulmonary vascular cells, including ECs and smooth muscle cells(16–18). In addition, peroxynitrite modifies amino acids resulting in tyrosine nitration of proteins (formation of 3-nitrotyrosine) and thus modifies their functions (14, 15). Peroxynitrite levels are elevated in the lung of patients with PAH (12, 13) , which are in part due to tissue hypoxia and inflammation (16, 17). Immunohistochemical staining show ubiquitous and marked increase of 3-nitrotyrosine (12). Our previous studies showed that Caveolin-1 (Cav1) deficiency results in eNOS activation and a marked increase of nitric oxide levels, as well as augmented production of superoxide, which form peroxynitrite leading to prominent nitrative stress in pulmonary vasculature (19–21). The resultant augmentation of nitrative stress causes protein kinase G (PKG) tyrosine nitration and impairs its kinase activity, leading to enhanced vasoconstriction and vascular remodeling and thus PH as seen in *Prkg*$^{-/-}$(*Prkg* encoding PKG) mice (20–22). PKG tyrosine nitration was markedly increased in the lungs of IPAH patients (20, 23).

Recently, we have reported the unprecedented mouse model of PAH [*Tie2Cre*-mediated disruption of *Egln1*, encoding hypoxia inducible factor (HIF) prolyl hydroxylase 2 (PHD2), designated *Egln1*$^{Tie2Cre}$] with progressive obliterative vascular remodeling including vascular occlusion and plexiform-like lesion and right heart failure, which recapitulates many features of clinical PAH including IPAH(24, 25). It is unknown whether oxidative/nitrative stress is also augmented and involved in the pathogenesis of PAH in this severe PAH model. In the present study, we found that nitrative stress and Cav1 deficiency are present in *Egln1*$^{Tie2Cre}$ mice in a HIF-2α

dependent manner. ROS scavenger treatment or restoration of endothelial Cav1 expression attenuated PAH in *Egln1*$^{Tie2Cre}$ mice.

## Methods

### Animal Models

All the mice used in this study are C57BL/6J background or backcrossing to C57BL/6J mice for more than 6 generation. *Egln1*$^{Tie2Cre}$ and *Hif2a*/*Egln1*$^{Tie2Cre}$ (EH2) mice were generated as described previously(24). *Cav1*$^{EC\text{-}Tg}$ mice were obtained from Dr. William Sessa's lab from Yale University, *Cav1*$^{EC\text{-}Tg}$ mice were generated by using SpeI-linearized 9.2-kb prepro- endothelin-1 promoter to drive the Cav-1 transgene.(26). *Egln1*$^{Tie2Cre}$ mice were bred with *Cav1*$^{EC\text{-}Tg}$ mice to generate *Egln1*$^{Tie2Cre}$/*Cav1*$^{EC\text{-}Tg}$ (CKO/Tg) mice. Both male and female *Egln1*$^{f/f}$ (designed as WT), *Egln1*$^{Tie2Cre}$, *Egln1*$^{Tie2Cre}$/*Cav1*$^{EC\text{-}Tg}$(CKO/Tg), and *Cav1*$^{EC\text{-}Tg}$ little mates at the age of 2~3.5 months were used in this studies. For ROS scavenger treatment, both male and female *Egln1*$^{Tie2Cre}$ mice at the age of 5 weeks were treated with manganese (III) tetrakis (1-methyl-4-pyridyl) porphyrin pentachloride (MnTmPyP) (5 mg/kg) (20) intraperitoneally daily for 9 weeks. PBS was used as a control. The animal care and study protocols were reviewed and approved by the Institutional Animal Care and Use Committees of the University of Illinois at Chicago, Northwestern University, and the University of Arizona.

### Echocardiography

Echocardiography was performed in the Core facility at the University of Illinois at Chicago and the University of Arizona as described previously(24, 27, 28). Transthoracic echocardiography was performed on a VisualSonics Vevo 2100 or 3100 ultrasound machine (FujiFilm VisualSonics Inc) using an MS550D (40 MHz) transducer. The right ventricle wall thickness during diastole (RVWTD) and the RV

cross-sectional area were obtained from the parasternal short axis view at the papillary muscle level using M-mode. Pulmonary artery (PA) acceleration time and PA ejection time were obtained from the parasternal short axis view at the aortic valve level using pulsed Doppler mode.

**Hemodynamics measurement**

In order to measure the right ventricular systolic pressure (RVSP), mice were anesthetized with Ketamine/Xylazine cocktail. A 1.4F pressure transducer catheter (Millar Instruments) was inserted through the right jugular vein into the right ventricle. RVSP was recorded and analyzed by AcqKnowledge software (Biopac Systems Inc.) as described previously(24, 27, 28).

**Endothelial cells isolation**

Mouse lung tissues were well-perfused with PBS to remove blood. The tissues were then minced and incubated with collagenase A (1.0 mg/ml in HBSS, Roche) in water bath shaker at 37℃ for 45 mins. The tissues were dispersed by gentleMACS Dissociator (Miltenyi Biotec), followed by filtering through a 40 μm cell strainer. Cells were then incubated with anti-mouse CD31 antibody (BD, cat#550274, 1.5 μg/ml) on ice for 1 hour and followed by incubation with sheep anti-rat IgG Dynabeads M-450 (Invitrogen, Cat#11035, 50 μl) for 30 mins. Beads bound ECs ($CD31^+$ cells) were pulled down by magnet (27, 28) and lysed for protein isolation.

**Histological assessment**

Mouse lung tissues were perfused with PBS and fixed with 10% formalin via tracheal instillation at a constant pressure (15 cm $H_2O$) and embedded in paraffin wax. Lung sections were stained with a Russel-Movat pentachrome staining kit (American MasterTech) according to the manufacturer's protocols. For assessment of PA wall thickness, PAs from 40 images at 20X magnification were quantified by Image J. Wall

thickness was calculated by the distance between internal wall and external wall divided by the distance between external wall and the center of lumen (24, 27, 28).

**Immunofluorescent staining**

Mouse lung tissues were perfused with PBS, inflated with 50% OCT in PBS, and embedded in OCT for cryosectioning. For immunofluorescent staining of Cav1 and α-nitrotyrosine (NT) (20), lung sections (5 μm) were fixed with 4% paraformaldehyde and blocked with 0.1% Triton X-100 and 5% normal goat serum at room temperature for 1 hour. After 3 washes with PBS, the slides were incubated with anti-Cav1 (Santa Cruz Biotechnology, Cat#sc-894, 1:100) or anti-NT (Millipore, Cat#05-233,1:300), anti-CD31 antibody (BD Bioscience, Cat#550274, 1:25), anti- α-SMA (Abcam, Cat#Ab5694, 1:300), anti-CD45 (Invitrogen, Cat# 14-0451-82, 1:100), anti-Periostin (Abcam, Cat#14041, 1:100) at 4°C overnight then incubated with Alexa 594-conjugated anti-mouse IgG, Alexa 488-conjugated anti-rat or anti-rabbit IgG (Life Technology) at room temperature for 1 h. Nuclei were counterstained with DAPI contained in Prolong Gold mounting media (Life Technology).

**RNA isolation and quantitative RT-PCR analysis**

One lobe of lung tissue was homogenized by a TissueLyser (Qiagen) in Trizol solution (Life Technology). RNA was isolated by phenol:chloroform, followed by cleanup with Qiagen RNA mini kit (Qiagen). One microgram of RNA was transcribed into cDNA using the high-capacity cDNA reverse transcription kits (Applied Biosystems). Quantitative RT-PCR analysis was performed on an ABI ViiA 7 Real-time PCR system (Applied Biosystems) with the FastStart SYBR Green Master kit (Roche Applied Science). Target mRNA expression was determined using the comparative cycle threshold method of relative quantitation. Cyclophilin A was used as an internal control. Information for mouse Cav1 and Cyclophilin A primers was described previously(24).

**Western Blotting**

Western blotting was performed using anti-Cav1 (Santa Cruz Biotechnology, Cat#sc-894, 1:2000), anti-NT (Millipore, Cat#05-233, 1:2000). Anti-β-actin (Sigma, Cat #A2228, 1:10,000) was used as a loading control.

**Measurement of reactive oxygen/nitrogen species (ROS/RNS) levels**

Lung tissues were perfused free of blood with PBS, followed by collection of left lobe. Fifty mg of lung tissue was homogenized in PBS on ice. Tissue homogenates were span at 10,000g for 5 min in 4 ℃. Fifty ul of homogenates were then used for determination of tissue ROS/RNS levels (OxiSelect™ In Vitro ROS/RNS Assay Kit, Cat#STA-347-T) according to the manufacture's guide. Samples and 2', 7'-dichlorodihydrofluorescein (DCF) were measured fluorometrically against DCF standards on a fluorescence plate reader (TECAN Infinite 200 Pro). The free radical content in homogenates is determined by comparison with the predetermined 2', 7'-dichlorodihydrofluorescein (DCF) standard curve. The relative DCF value was normalized by the mean value of WT group.

**Statistical analysis**

Statistical significance was determined by one-way ANOVA with a Tukey post hoc analysis that calculates P values corrected for multiple comparisons. Two-group comparisons were analyzed by the unpaired 2-tailed Student t-test for equal variance or the Welch t-test for unequal variance. $P < 0.05$ denoted the presence of a statistically significant difference. All bar graphs represent mean ± SD.

## Results

**Prominent nitrative stress in *Egln1*$^{Tie2Cre}$ mouse lungs**

Given that nitrative stress is a characteristic feature of the pathology of clinical PAH, we tested whether nitrative stress is also prominent in the lung of *Egln1*$^{Tie2Cre}$ mice. Quantification of total free radical levels with the OxiSelect™ *In Vitro* ROS/RNS

Assay Kit of lung homogenates showed that *Egln1*$^{Tie2Cre}$ lungs exhibited markedly elevated ROS/RNS levels (**Figure 1A**). Western blotting demonstrated that nitrotyrosine (NT) expression, indicative of nitrative stress (16), was strongly induced in *Egln1*$^{Tie2Cre}$ mouse lungs (**Figure 1B** and **1C**). We then performed the NT staining together with ECs (CD31), inflammatory cells (CD45), fibroblasts (periostin), smooth muscle cells (α-SMA) markers and to determine what cell types are the NT positive cells in the lung of *Egln1*$^{Tie2Cre}$ mice. Our data showed that NT is highly expressed in the EC, CD45$^{+}$ inflammatory cells and relatively lower expression in the α-SMA smooth muscle cells and periostin$^{+}$ fibroblasts (**Figure 1D-1E and supplemental Figure 1A and 1B**). Our previous studies demonstrated that nitration–dependent impairment of PKG activity is involved in PH development(29). To further determine whether PHD2 deficiency also affects PKG nitration and expression, we performed immunoprecipitation assay using anti-PKG antibodies and blotted with anti-NT antibodies. The data showed that PKG nitration was markedly increased in the lung of *Egln1*$^{Tie2Cre}$ mice (**Supplemental Figure 1C**). Together, these data suggest that nitrative stress is markedly augmented in the pulmonary vascular lesions in *Egln1*$^{Tie2Cre}$ mice.

**ROS scavengers inhibit PAH in *Egln1*$^{Tie2Cre}$ mice**

We next determined whether removing ROS in *Egln1*$^{Tie2Cre}$ mice will affect the development of PAH. *Egln1*$^{Tie2Cre}$ mice at age of 5-weeks were treated with the ROS scavenger MnTMPyP (a superoxide dismutase mimetic) (20, 30) via i.p. injection for 9 weeks. MnTMPyP treatment reduced the levels of NT in the pulmonary vasculature and lung of *Egln1*$^{Tie2Cre}$ mice (**Figure 2A**). Hemodynamics measurement and cardiac dissection showed that RVSP and RV hypertrophy were partially reduced by MnTMPyP treatment in *Egln1*$^{Tie2Cre}$ mice (**Figure 2B** and **2C**). Lung pathology examination also revealed inhibition of occlusive vascular remodeling evident by diminished neointima formation (**Figure 3A**), and decreased pulmonary arterial wall thickness and muscularization of distal pulmonary vessels in MnTMPyP-treated *Egln1*$^{Tie2Cre}$ mice compared to PBS treated mice (**Figure 3B-3E**). To scavenger NO, we

treated *Egln1*$^{Tie2Cre}$ mice at the age of 5 weeks with NOS inhibitor L-NAME. However, the *Egln1*$^{Tie2Cre}$ mice died after ~7 days treatment (data not shown), suggested that NO is very important to maintain the vascular homeostasis. Together, these data suggest the involvement of oxidative/nitrative stress in severe PAH in *Egln1*$^{Tie2Cre}$ mice.

**Decreased expression of endothelial Caveolin-1 secondary to PHD2 deficiency in a HIF-2α dependent manner**

Cav1 deficiency increases ROS and RNS production, leading to nitrative stress, which post-translationally modifies PKG through tyrosine nitration and impairs its kinase activity leading to PH(20, 21). To find out whether dysregulation of Cav1 signaling is involved in the generation of nitrative stress and PAH development in *Egln1*$^{Tie2Cre}$ mice, we first checked the expression level of Cav1 in the lungs of *Egln1*$^{Tie2Cre}$ mice. As shown in **Figure 4A**, *Cav1* mRNA levels was markedly decreased in the lungs of *Egln1*$^{Tie2Cre}$ mice compared to that from similar age *Egln1*$^{f/f}$ (WT) mice. HIF-2α deletion restored the expression of *Cav1* mRNA (**Figure 4A**). Western blotting also demonstrated reduced Cav1 protein levels in *Egln1*$^{Tie2Cre}$ mouse lungs which were reversed in *Egln1*$^{Tie2Cre}$/*Hif2a*$^{Tie2Cre}$ (EH2) mice and in fact increased in EH2 mouse lungs compared to WT lungs (**Figure 4B** and **4C, Supplemental Figure 2**). By performing immunofluorescent staining, we found that Cav1 is co-stained with CD31$^{+}$ cells in the pulmonary vasculature of WT mice and diminished in vascular lesions in *Egln1*$^{Tie2Cre}$ mice whereas restored in CD31$^{+}$ cells in the pulmonary vasculature of EH2 mice (**Figure 4D**), suggesting that endothelial Cav1 is reduced by PHD2 deficiency dependent on HIF-2α activation in *Egln1*$^{Tie2Cre}$ mice.

**Restored Cav1 expression normalized nitrative stress in *Egln1*$^{Tie2Cre}$ mice**

To determine whether Cav1 deficiency is responsible for the augmentation of nitrative stress and the pathogenesis of PAH in *Egln1*$^{Tie2Cre}$ mice, we generated a mouse model with Cav1 transgenic expression in ECs in the background of *Egln1*$^{Tie2Cre}$ mice (*Egln1*$^{Tie2Cre}$/Cav1$^{EC\text{-}Tg}$, *CKO/Tg*)(31) (**Figure 5A**). Western blotting and immunostaining demonstrated that reduced Cav1 expression seen in *Egln1*$^{Tie2Cre}$ mouse lungs was normalized in *CKO/Tg* mice (**Figure 5B and 5C**). Restored Cav1 expression

in ECs in *Egln1*$^{Tie2Cre}$ mice drastically reduced the levels of ROS/RNS in the lung of *Egln1*$^{Tie2Cre}$ mice (**Figure 6A**). Further examination of NT expression via Western Blotting and immunostaining showed that NT levels were inhibited in the lung and pulmonary ECs of *CKO/Tg* mice compared to *Egln1*$^{Tie2Cre}$ mice, suggesting that Cav1 deficiency is responsible for the increased nitrative stress in *Egln1*$^{Tie2Cre}$ mouse lungs.

**Cav1 transgenic expression inhibits PAH in *Egln1*$^{Tie2Cre}$ mice**

We next determined if Cav1 transgenic expression in *Egln1*$^{Tie2Cre}$ mice will rescue the hypertensive pulmonary phenotype. Hemodynamic measurement demonstrated a partial decrease of RVSP in *CKO/Tg* at age of 3.5 months compared to *Egln1*$^{Tie2Cre}$ mice (**Figure 7A**). RV hypertrophy, determined by weight ratio of RV versus left ventricular plus septum (LV+S) was also partially attenuated in *CKO/Tg* mice compared to *Egln1*$^{Tie2Cre}$ mice (**Figure 7B**). Pathological examination showed that *CKO/Tg* mice had reduced pulmonary vascular remodeling, including decreases of neointima and occlusive lesions, pulmonary arterial wall thickness, and muscularization of distal pulmonary vessels in comparison of *Egln1*$^{Tie2Cre}$ mice (**Figure 7C-7F**).

**Cav1 transgenic expression increased RV contractility in *Egln1*$^{Tie2\mathrm{Cre}}$ mice**

We next evaluate whether Cav1 transgenic expression will inhibit right heart dysfunction seen in *Egln1*$^{Tie2Cre}$ mice. As shown in **Figure 8A-7C**, echocardiography showed that *CKO/Tg* mice had marked decreases of RV wall thickness and RV chamber size compared to *Egln1*$^{Tie2Cre}$ mice. *CKO/Tg* mice also exhibited marked improvements of RV contractility assessed by RV fraction area change compared to *Egln1*$^{Tie2Cre}$ mice (**Figure 8D and Supplemental Video 1-2**). However, we did not observe significant change of heart rate, cardiac output and left ventricular fraction shorting in *CKO/Tg* mice compared with *Egln1*$^{Tie2Cre}$ mice (**Supplemental Figure 3A-3C**). PA function assessed by PA acceleration time/ejection time (AT/ET) showed that CKO/Tg mice exhibited improved PA function compared to *Egln1*$^{Tie2Cre}$ mice (**Figure 8E**). These data demonstrated that endothelial Cav1 transgenic expression partially but significantly rescues the defective PA and RV functions seen in *Egln1*$^{Tie2\mathrm{Cre}}$ mice.

## Discussion

The present study demonstrated that nitrative stress was markedly augmented in the lungs, especially in vascular lesions of *Egln1*$^{Tie2Cre}$ mice, recapitulating the pathological feature of clinical PAH. Augmentation of nitrative stress was due to endothelial Cav1 deficiency. Endothelial Cav1 transgenic expression in *Egln1*$^{Tie2Cre}$/*Cav1*Tg mice reduced nitrative stress levels and attenuated PAH evident by reduction of RVSP, pulmonary vascular remodeling, and RV hypertrophy, as well as improvements of RV and PA function. We also observed that pharmacological scavenging of ROS markedly reduced the severity of pulmonary vascular remodeling and PAH in *Egln1*$^{Tie2Cre}$ mice. These findings suggest that restoration of Cav1 expression in ECs and ROS scavenger represent therapeutic strategies for the treatment of severe PAH, including IPAH (**Figure 8F**).

Prominent oxidative/nitrative stress is a pathological feature of clinical PAH(16, 17). Our recent study has for the first time shown that *Egln1*$^{Tie2Cre}$ mice develop spontaneously severe PAH with obliterative pulmonary vascular remodeling including occlusive vascular lesions and formation of plexiform-like lesions and marked elevation of RVSP ranging from 70-100 mmHg as well as development of right heart failure (24). Here we show a marked increase of ROS/RNS in *Egln1*$^{Tie2Cre}$ mouse lungs and prominent anti-NT staining indicative of nitrative stress in pulmonary vascular lesions. This study provides further evidence of *Egln1*$^{Tie2Cre}$ mice as an excellent mouse model of human PAH. Furthermore, treatment of the mice with the ROS scavenger MnTMPyP inhibited occlusive pulmonary vascular remodeling and attenuated PAH, demonstrating the pathogenic role of oxidative/nitrative stress in contributing to the severity of PAH.

Previous studies have shown decreases of *CAV1* mRNA and protein levels in lung ECs of patients with PAH(20, 30, 31). Cav1 deficiency is also evident in the arterial lesions of PAH rats including both Sugen5416/hypoxia-induced PAH and monocrotaline-induced PAH(33, 34). Our previous study provides the first genetic

evidence that Cav1 deficiency induces PH in mice (19). Others also observe pulmonary defects in *Cav1*$^{-/-}$ mice (35). A recent study shows that Cav1 deficiency in ECs promote more severe PH in response to hypoxia (36). Consistently, *CAV1* mutation is associated with heritable PAH in patients (37). Together, these studies provide unequivocal evidence of CAV1 deficiency in the pathogenesis of PAH. Our other study has shown that mice with genetic deletions of both *Cav1* and *Nos3* or treatment of *Cav1*$^{-/-}$ mice with either NOS inhibitor L-NAME or ROS scavenger MnTMPyP inhibited PAH, suggesting chronic activation of eNOS secondary to Cav1 deficiency is the mechanism of PAH induced by CAV1 deficiency (20). Others also show that L-NAME treatment inhibits PH in *Cav1*$^{-/-}$ mice (38). eNOS activation-derived NO reacts with superoxide to form the damaging peroxynitrite which causes posttranslational modification of proteins such as PKG via tyrosine nitration in *Cav1*$^{-/-}$ mice. PKG nitration impairs its kinase activity and thereby induces pulmonary vascular remodeling and PH (20, 22). Accordingly, *Prkg1*$^{-/-}$ (i.e., PKG deficiency) mice exhibit PH (22). PKG nitration is prominent in lung tissues of IPAH patients (20, 23). Thus, Cav1 deficiency induces nitrative stress leading to PKG nitration and PH.

In *Egln1*$^{Tie2\mathrm{Cre}}$ mice, we observed elevated levels of ROS/RNS, PKG nitration and decrease of endothelial Cav1 expression. We demonstrated that Cav1 deficiency in *Egln1*$^{Tie2\mathrm{Cre}}$ mice is involved in the regulation of nitrative stress level as endothelial Cav1 transgenic expression normalizes the levels of ROS/RNS and thus inhibits obliterative pulmonary vascular remodeling and reduces PAH as well as improves RV function in *Egln1*$^{Tie2\mathrm{Cre}}$ mice. Especially, we observed complete inhibition of occlusive vascular remodeling without neointima formation in both *Egln1*$^{Tie2\mathrm{Cre}}$/*Cav1*Tg mice and MnTMPyP-treated *Egln1*$^{Tie2\mathrm{Cre}}$ mice. The medial thickness was less affected in these mice, which is consistent with the markedly reduced but still elevated RVSP. Together, our data demonstrate that Cav1 deficiency mediates the augmentation of nitrative stress in *Egln1*$^{Tie2\mathrm{Cre}}$ mice and contributes to the severity of PAH.

Given the limitation that both *Egln1*$^{Tie2\mathrm{Cre}}$ mice and Cav1 Tg mice are not conditional, thus the effects of these transgenic manipulations would be exerted

throughout developmental stage. It is possible that the phenotype may reflect effects on embryonic vascular development. Since PAH is a disease that occurs mainly in adults (and less commonly in children), future studies are warranted to address these mechanisms using similar manipulations postnatally.

In summary, we have demonstrated prominent nitrative stress in vascular lesions of *Egln1*$^{Tie2\mathrm{Cre}}$ mice, which is mediated by endothelial Cav1 deficiency. ROS scavenger treatment or transgenic expression of Cav1 inhibits obliterative pulmonary vascular remodeling and attenuates PAH in *Egln1*$^{Tie2\mathrm{Cre}}$ mice. Thus, Cav1 deficiency-induced oxidative/nitrative stress secondary to *Egln1* deficiency and resultant HIF-2α activation is a part of the mechanisms of severe PAH in *Egln1*$^{Tie2\mathrm{Cre}}$ mice as seen in PAH patients.

**Acknowledgement**

We greatly appreciate Dr. William C. Sessa from the Departments of Pharmacology, and Medicine at Yale School of Medicine for his generosity of providing us the *Cav1*$^{EC-Tg}$ mice.

**Author contributions**

Z.D. and Y.Y.Z. conceived the experiments. Z.D., J.D., B.L., D. Y., Y. P. and M.M.Z designed, carried out experiments, and analyzed the data. Z.D., R.V. and Y.Y.Z. analyzed and interpreted the data. Z.D. wrote the manuscript. Z.D. and Y.Y.Z. supervised the project and revised the manuscript.

**Sources of Funding**

This work was supported in part by NIH grants R01HL123957, R01HL125350, R01HL133951, R01HL140409 and P01HL077806 (Project 3) to Y.Y.Z, and NIH R00HL13827, AHA Career Development Award, ATS Foundation Pulmonary Hypertension Association Research Fellowship, Arizona Biomedical Research Centre funding (ADHS18-198871)，the University of Arizona departmental Startup funding to Z.D.

**Reference**


1. McLaughlin V V., Archer SL, Badesch DB, Barst RJ, Farber HW, Lindner JR, Mathier MA, McGoon MD, Park MH, Rosenson RS, Rubin LJ, Tapson VF, Varga J. A report of the american college of cardiology foundation task force on expert consensus documents and the american heart association. *Circulation* 2009;119:2250–2294.

2. Hoeper MM, Bogaard HJ, Condliffe R, Frantz R, Khanna D, Kurzyna M, Langleben D, Manes A, Satoh T, Torres F, Wilkins MR, Badesch DB. Definitions and diagnosis of pulmonary hypertension. *J Am Coll Cardiol* 2013;62:D42–D50.

3. Thenappan T, Ormiston ML, Ryan JJ, Archer SL. Pulmonary arterial hypertension: Pathogenesis and clinical management. *BMJ* 2018;360:j5492.

4. Humbert M, Guignabert C, Bonnet S, Dorfmüller P, Klinger JR, Nicolls MR, Olschewski AJ, Pullamsetti SS, Schermuly RT, Stenmark KR, Rabinovitch M. Pathology and pathobiology of pulmonary hypertension: state of the art and research perspectives. *Eur Respir J* 2019;53:1801887.

5. Stacher E, Graham BB, Hunt JM, Gandjeva A, Groshong SD, McLaughlin V V., Jessup M, Grizzle WE, Aldred MA, Cool CD, Tuder RM. Modern age pathology of pulmonary arterial hypertension. *Am J Respir Crit Care Med* 2012;186:261–272.

6. Sutendra G, Michelakis ED. Pulmonary Arterial Hypertension: Challenges in Translational Research and a Vision for Change. *Sci Transl Med* 2013;5:208sr5-208sr5.

7. Wilkins MR, Aman J, Harbaum L, Ulrich A, Wharton J, Rhodes CJ. Recent advances in pulmonary arterial hypertension. *F1000Research* 2018;7:1128.

8. McLaughlin V V, Shah SJ, Souza R, Humbert M. Management of pulmonary

arterial hypertension. *J Am Coll Cardiol* 2015;65:1976–1997.

9. Pullamsetti SS, Schermuly R, Ghofrani A, Weissmann N, Grimminger F, Seeger W. Novel and Emerging Therapies for Pulmonary Hypertension. *Am J Respir Crit Care Med* 2014;189:394–400.

10. Spiekermann S, Schenk K, Hoeper MM. Increased xanthine oxidase activity in idiopathic pulmonary arterial hypertension. *Eur Respir J* 2009;34:276–276.

11. Jankov RP, Kantores C, Pan J, Belik J. Contribution of xanthine oxidase-derived superoxide to chronic hypoxic pulmonary hypertension in neonatal rats. *Am J Physiol Cell Mol Physiol* 2008;294:L233–L245.

12. Bowers R, Cool C, Murphy RC, Tuder RM, Hopken MW, Flores SC, Voelkel NF. Oxidative Stress in Severe Pulmonary Hypertension. *Am J Respir Crit Care Med* 2004;169:764–769.

13. Masri FA, Comhair SAA, Dostanic-Larson I, Kaneko FT, Dweik RA, Arroliga AC, Erzurum SC. Deficiency of Lung Antioxidants in Idiopathic Pulmonary Arterial Hypertension. *Clin Transl Sci* 2008;1:99–106.

14. Beckman JS, Beckman TW, Chen J, Marshall PA, Freeman BA. Apparent hydroxyl radical production by peroxynitrite: implications for endothelial injury from nitric oxide and superoxide. *Proc Natl Acad Sci U S A* 1990;87:1620–4.

15. Beckman JS, Koppenol WH. Nitric oxide, superoxide, and peroxynitrite: the good, the bad, and ugly. *Am J Physiol* 1996;271:C1424-37.

16. Evans CE, Zhao Y-Y. Molecular Basis of Nitrative Stress in the Pathogenesis of Pulmonary Hypertension. *Adv Exp Med Biol* 2017;967:33–45.

17. Fulton D, Li X, Bordan Z, Haigh S, Bentley A, Chen F, Barman S. Reactive Oxygen and Nitrogen Species in the Development of Pulmonary Hypertension. *Antioxidants* 2017;6:54.

18. Aggarwal S, Gross CM, Sharma S, Fineman JR, Black SM. Reactive oxygen

species in pulmonary vascular remodeling. *Compr Physiol* 2013;3:1011–1034.

19. Zhao Y-Y, Liu Y, Stan R-V, Fan L, Gu Y, Dalton N, Chu P-H, Peterson K, Ross J, Chien KR. Defects in caveolin-1 cause dilated cardiomyopathy and pulmonary hypertension in knockout mice. *Proc Natl Acad Sci* 2002;99:11375–11380.

20. Zhao Y-Y, Zhao YD, Mirza MK, Huang JH, Potula H-HSK, Vogel SM, Brovkovych V, Yuan JX-J, Wharton J, Malik AB. Persistent eNOS activation secondary to caveolin-1 deficiency induces pulmonary hypertension in mice and humans through PKG nitration. *J Clin Invest* 2009;119:2009–2018.

21. Zhao Y-Y, Malik AB. A novel insight into the mechanism of pulmonary hypertension involving caveolin-1 deficiency and endothelial nitric oxide synthase activation. *Trends Cardiovasc Med* 2009;19:238–242.

22. Zhao YD, Cai L, Mirza MK, Huang X, Geenen DL, Hofmann F, Yuan JX-J, Zhao YY. Protein kinase G-I deficiency induces pulmonary hypertension through Rho A/Rho kinase activation. *Am J Pathol* 2012;180:2268–2275.

23. Aggarwal S, Gross CM, Rafikov R, Kumar S, Fineman JR, Ludewig B, Jonigk D, Black SM. Nitration of Tyrosine 247 Inhibits Protein Kinase G-1α Activity by Attenuating Cyclic Guanosine Monophosphate Binding. *J Biol Chem* 2014;289:7948–7961.

24. Dai Z, Li M, Wharton J, Zhu MM, Zhao YY. Prolyl-4 Hydroxylase 2 (PHD2) deficiency in endothelial cells and hematopoietic cells induces obliterative vascular remodeling and severe pulmonary arterial hypertension in mice and humans through hypoxia-inducible factor-2α. *Circulation* 2016;133:2447–2458.

25. Dai Z, Zhao Y-YY-Y. Discovery of a murine model of clinical PAH: Mission impossible? *Trends Cardiovasc Med* 2017;27:229–236.

26. Bauer PM, Yu J, Chen Y, Hickey R, Bernatchez PN, Looft-Wilson R, Huang

Y, Giordano F, Stan R V., Sessa WC. Endothelial-specific expression of caveolin-1 impairs microvascular permeability and angiogenesis. *Proc Natl Acad Sci U S A* 2005;102:204–209.

27. Dai Z, Zhu MM, Peng Y, Machireddy N, Evans CE, Machado R, Zhang X, Zhao YY. Therapeutic targeting of vascular remodeling and right heart failure in pulmonary arterial hypertension with a HIF-2a inhibitor. *Am J Respir Crit Care Med* 2018;198:1423–1434.

28. Dai Z, Zhu MM, Peng Y, Jin H, Machireddy N, Qian Z, Zhang X, Zhao YY. Endothelial and smooth muscle cell interaction via FoxM1 signaling mediates vascular remodeling and pulmonary hypertension. *Am J Respir Crit Care Med* 2018;198:788–802.

29. Zhao Y-Y, Zhao YD, Mirza MK, Huang JH, Potula H-HSK, Vogel SM, Brovkovych V, Yuan JX-J, Wharton J, Malik AB. Persistent eNOS activation secondary to caveolin-1 deficiency induces pulmonary hypertension in mice and humans through PKG nitration. *J Clin Invest* 2009;119:2009–2018.

30. Peng YJ, Yuan G, Ramakrishnan D, Sharma SD, Bosch-Marce M, Kumar GK, Semenza GL, Prabhakar NR. Heterozygous HIF-1α deficiency impairs carotid body-mediated systemic responses and reactive oxygen species generation in mice exposed to intermittent hypoxia. *J Physiol* 2006;577:705–716.

31. Murata T, Lin MI, Huang Y, Yu J, Bauer PM, Giordano FJ, Sessa WC. Reexpression of caveolin-1 in endothelium rescues the vascular, cardiac, and pulmonary defects in global caveolin-1 knockout mice. *J Exp Med* 2007;204:2373–2382.

32. Geraci MW, Moore M, Gesell T, Yeager ME, Alger L, Golpon H, Gao B, Loyd JE, Tuder RM, Voelkel NF. Gene expression patterns in the lungs of patients with primary pulmonary hypertension: A gene microarray analysis. *Circ Res* 2001;88:555–562.

33. Achcar ROD, Demura Y, Rai PR, Taraseviciene-Stewart L, Kasper M, Voelkel

NF, Cool CD. Loss of caveolin and heme oxygenase expression in severe pulmonary hypertension. *Chest* 2006;129:696–705.

34. Mathew R, Huang J, Shah M, Patel K, Gewitz M, Sehgal PB. Disruption of endothelial-cell caveolin-1α/raft scaffolding during development of monocrotaline-induced pulmonary hypertension. *Circulation* 2004;110:1499–1506.

35. Razani B, Engelman JA, Wang XB, Schubert W, Zhang XL, Marks CB, Macalusol F, Russell RG, Li M, Pestell RG, Di Vizio D, Hou H, Kneitz B, Lagaud G, Christ GJ, Edelmann W, Lisanti MP. Caveolin-1 Null Mice Are Viable but Show Evidence of Hyperproliferative and Vascular Abnormalities. *J Biol Chem* 2001;276:38121–38138.

36. Oliveira SDS, Chen J, Castellon M, Mao M, Raj JU, Comhair S, Erzurum S, Silva CLM, Machado RF, Bonini MG, Minshall RD. Injury-Induced Shedding of Extracellular Vesicles Depletes Endothelial Cells of Cav-1 (Caveolin-1) and Enables TGF-β (Transforming Growth Factor-β)–Dependent Pulmonary Arterial Hypertension. *Arterioscler Thromb Vasc Biol* 2019;39:1191–1202.

37. Austin ED, Ma L, LeDuc C, Berman Rosenzweig E, Borczuk A, Phillips JA, Palomero T, Sumazin P, Kim HR, Talati MH, West J, Loyd JE, Chung WK. Whole exome sequencing to identify a novel gene (caveolin-1) associated with human pulmonary arterial hypertension. *Circ Cardiovasc Genet* 2012;5:336–343.

38. Wunderlich C, Schmeisser A, Heerwagen C, Ebner B, Schober K, Braun-Dullaeus RC, Schwencke C, Kasper M, Morawietz H, Strasser RH. Chronic NOS inhibition prevents adverse lung remodeling and pulmonary arterial hypertension in caveolin-1 knockout mice. *Pulm Pharmacol Ther* 2008;21:507–515.

## Figures

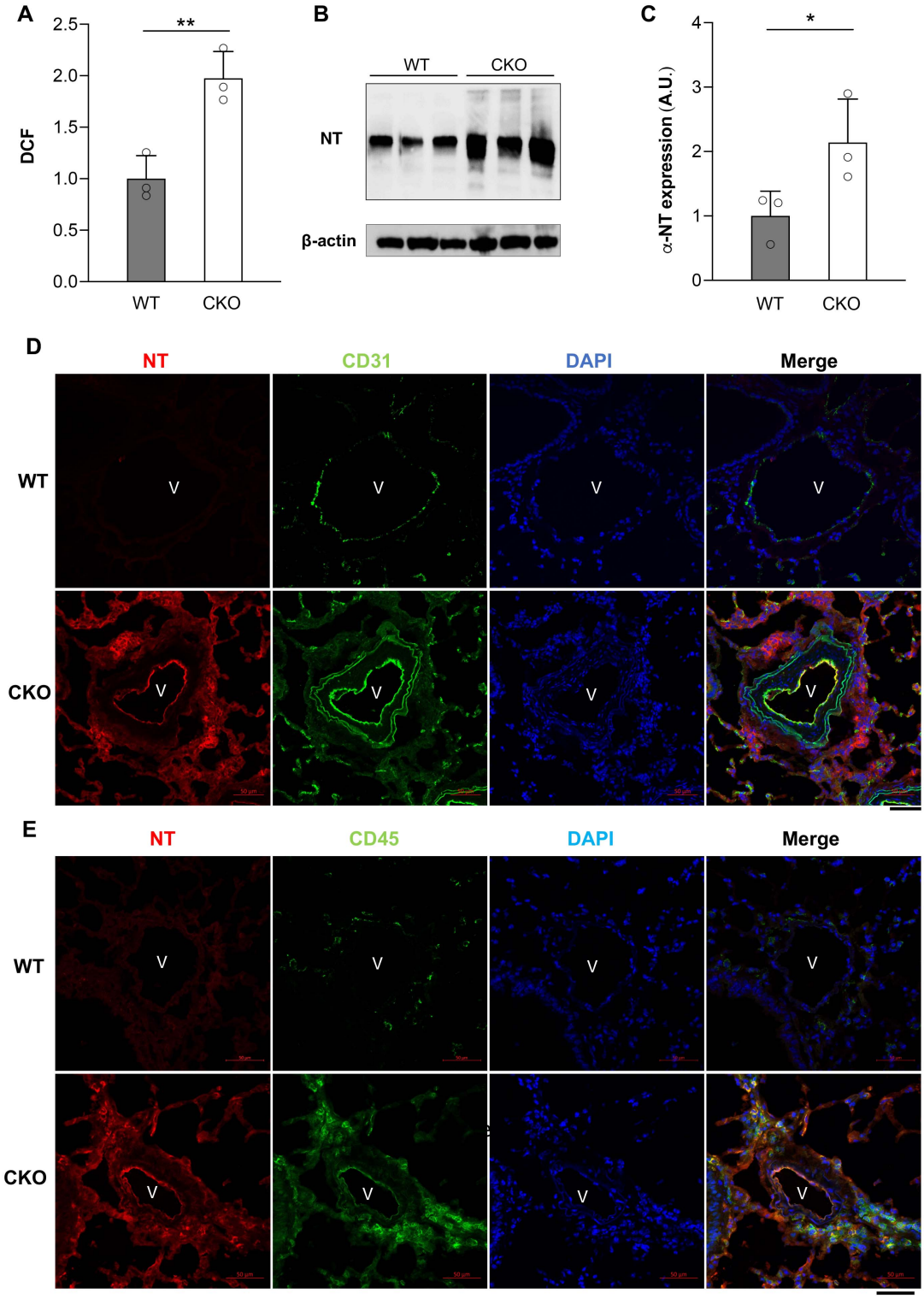


**Figure 1. Augmented nitrative stress in pulmonary vascular lesions in *Egln1*$^{Tie2Cre}$ mice.** (**A**) DCF measurement demonstrating marked increase of ROS/RNS in the lungs of *Egln1*$^{Tie2Cre}$ mice. Lung tissues were collected from 3.5 months old WT and

*Egln1*$^{Tie2Cre}$ mice for 2', 7'-dichlorodihydrofluorescein (DCF) assay. (**B**, **C**) Western blotting demonstrating increase of nitrotyrosine modification of proteins in the lung of *Egln1*$^{Tie2Cre}$ mice. NT, anti-NT antibody. (**D and E**) Representative micrographs of immunostaining showing prominent nitrative stress in pulmonary vascular lesions in *Egln1*$^{Tie2Cre}$ mice (3.5 months old). Lung sections were immunostained with anti-NT antibody (red) for detection of nitrative stress. Anti-CD31 antibodies were used to label vascular ECs (green, **D**). Anti-CD45 antibodies were used to label inflammatory cells (green, **E**). Nuclei were counterstained with DAPI (blue). V, vessel. Scale bar, 50 μm. *, $P < 0.05$. Welch t-test. (**A**, **C**).

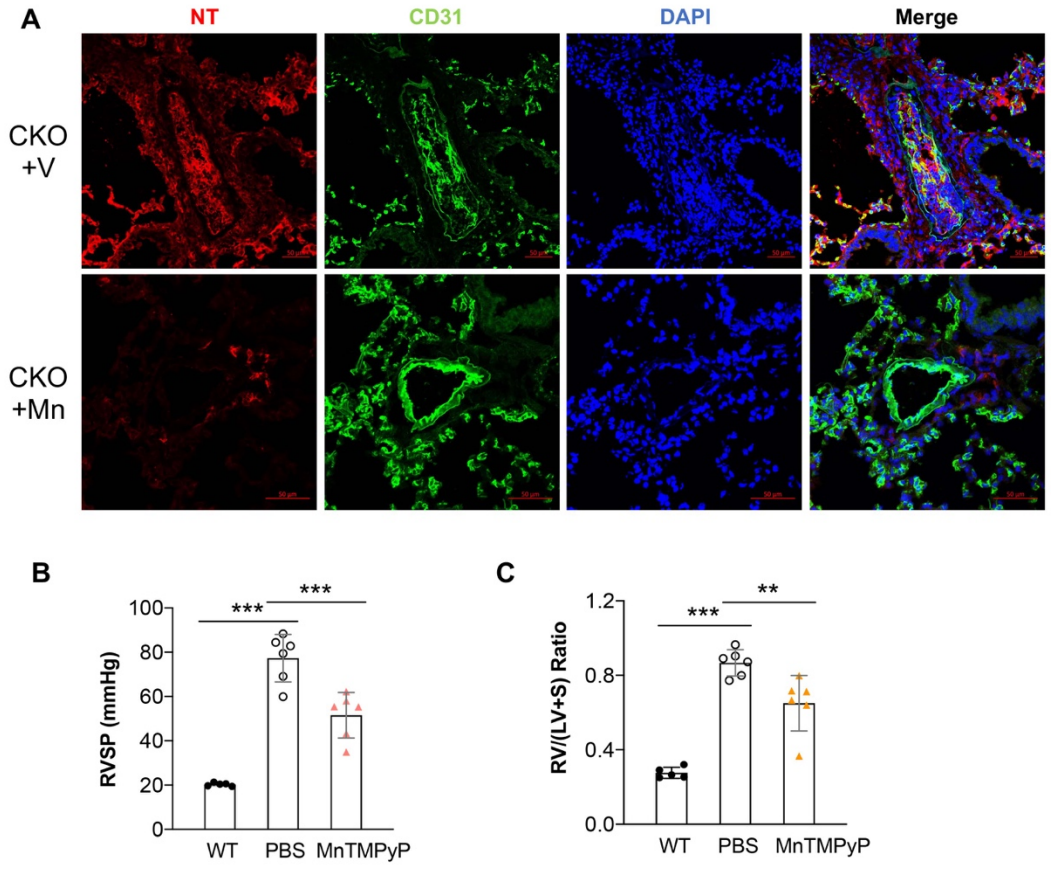


**Figure 2. MnTMPyP treatment reduced PAH in *Egln1$^{Tie2Cre}$* mice**. (**A**) Immunostaining against NT showed that MnTMPyP treatment reduced nitrotyrosine modification in *Egln1$^{Tie2Cre}$* (CKO) lung. *Egln1$^{Tie2Cre}$* mice at age of 5 weeks were treated with either MnTMPyP (Mn) or vehicle (PBS) for 9 weeks. (**B** and **C**) RVSP was measured and RV hypertrophy was determined in *Egln1$^{Tie2Cre}$* (CKO) mice treated with MnTMPyP. *Egln1$^{f/f}$* (WT) mice were used as controls. **, $P< 0.01$, ***, $P<0.001$. One-way ANOVA and Tukey post-hoc analysis (**B** and **C**).

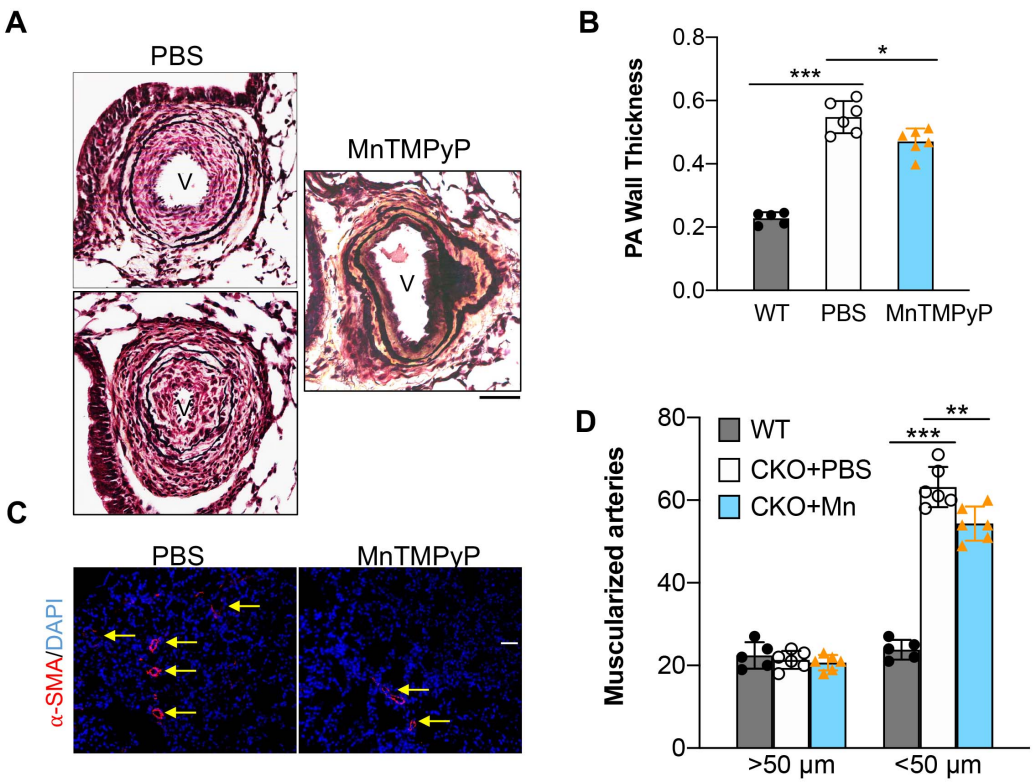


**Figure 3. MnTMPyP inhibited obliterative vascular remodeling in *Egln1*$^{Tie2Cre}$ mice**. (**A**, **B**) MnTMPyP treatment inhibited neointima formation and decreased PA wall thickness. Lung sections were processed for Russel-Movat pentachrome staining. V, vessel. (**C**, **D**) Quantification of α-SMA immunostaining demonstrating decreased muscularization of distal pulmonary vessels. Lung cryosections were immunostained with anti-α-SMA (red) and counterstained with DAPI (blue). Arrows point to muscularized distal pulmonary vessels. *, $P< 0.05$, **, $P< 0.01$, ***, $P<0.001$. One-way ANOVA and Tukey post-hoc analysis (**B** and **D**). Scale bar: 50μm.

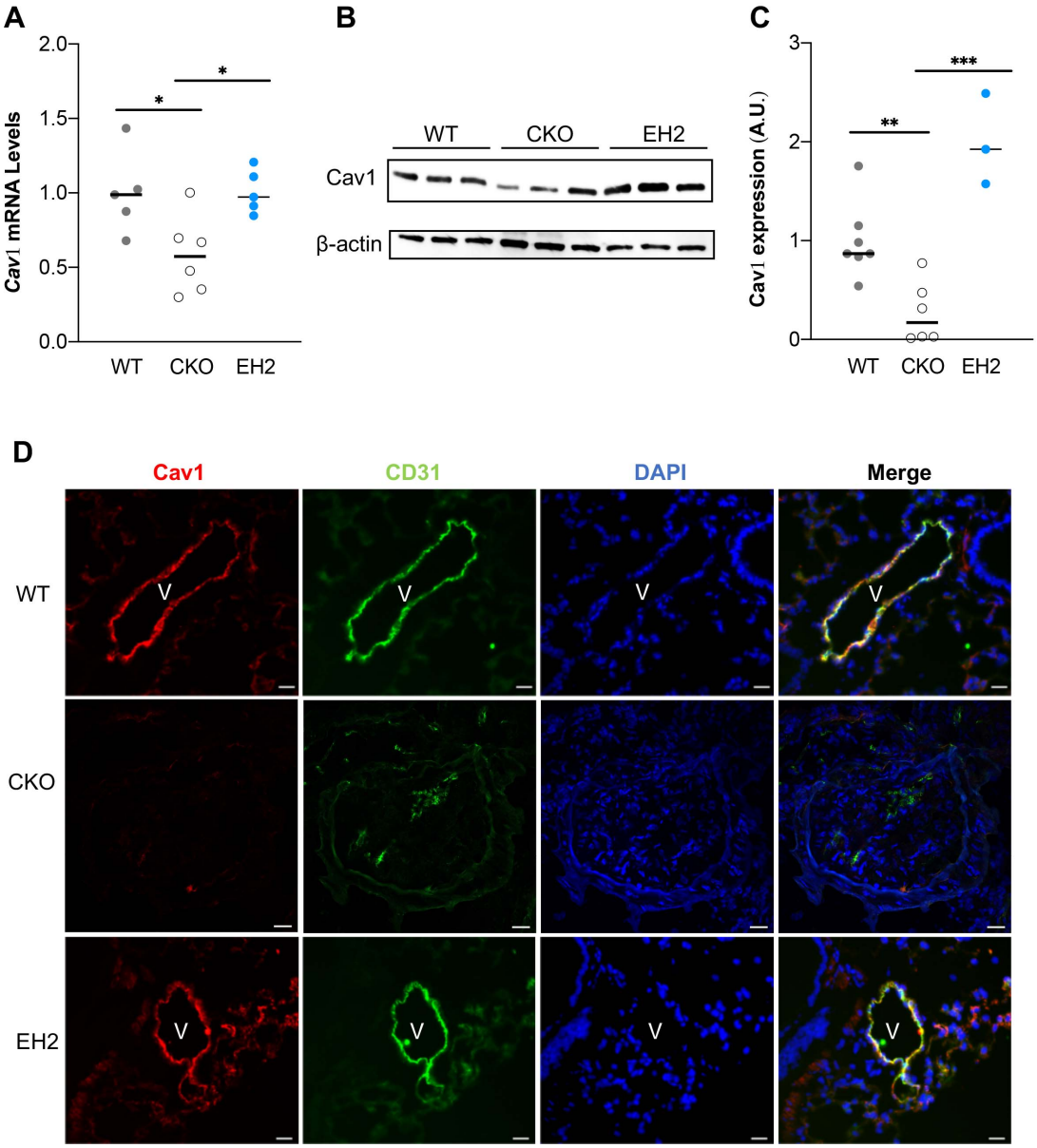


**Figure 4. Endothelial Cav1 expression was suppressed in *Egln1*$^{Tie2Cre}$ mouse lungs in a HIF-2α dependent manner.** (**A**) Quantitative RT-PCR analysis demonstrating decreased Cav1 mRNA expression in *Egln1*$^{Tie2Cre}$ (CKO) mouse lungs compared to WT lungs, which is restored in *Egln1*$^{Tie2Cre}$/*Hif2a*$^{Tie2Cre}$ (EH2) lungs. Lung tissues were collected from 3.5 months old mice. (**B**, **C**) Decreased Cav1 protein expression in *Egln1*$^{Tie2Cre}$ mouse lungs compared to WT lungs. Cav1 protein expression in EH2 mouse lungs was markedly increased compared to WT and *Egln1*$^{Tie2Cre}$ mouse lungs. (**D**) Immunostaining demonstrating diminished Cav1 expression in pulmonary vascular ECs of *Egln1*$^{Tie2Cre}$ mice and restoration in EH2 mice. Lung sections were

immunostained with anti-Cav1 (red) and CD31 (green). Nuclei were counterstained with DAPI (blue). *, $P< 0.05$, **, $P<0.01$. One-way ANOVA and Tukey post-hoc analysis (**A** and **C**). Scale bar: 50μm.

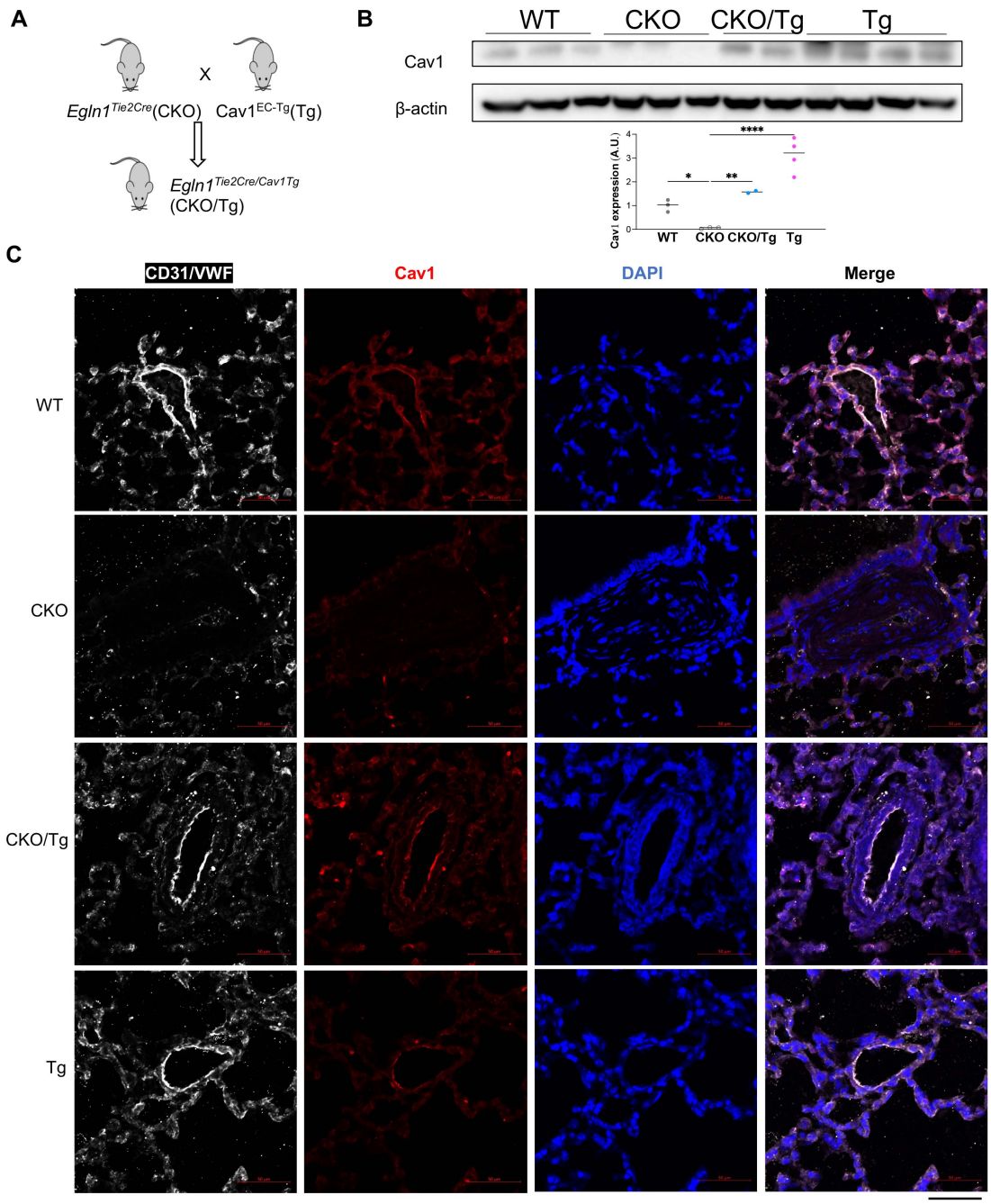


**Figure 5. Endothelial Cav1 transgenic expression in *Egln1*$^{Tie2Cre}$ mice.** (**A**) A diagram showing the strategy of generating *Egln1*$^{Tie2Cre}$/*Cav1*$^{EC\text{-}Tg}$ (CKO/Tg) mice by breeding endothelial Cav1 transgenic mice (*Cav1*$^{EC\text{-}Tg,}$ *Tg*) into the genetic background of *Egln1*$^{Tie2Cre}$ mice. (**B**) Western blotting demonstrating restored Cav1 expression in lung from CKO/Tg mice. (C) Immunostaining demonstrated that Cav1 expression was downregulated in lung ECs of *Egln1*$^{Tie2Cre}$ (CKO) mice compared to WT which was restored in CKO/Tg mice. Lung sections were immunostained with anti-Cav1 (red) and

CD31/VWF (white). Nuclei were counterstained with DAPI (blue). *, $P< 0.05$, **, $P<0.01$, ****, $P<0.0001$. One-way ANOVA and Tukey post-hoc analysis (**B**).

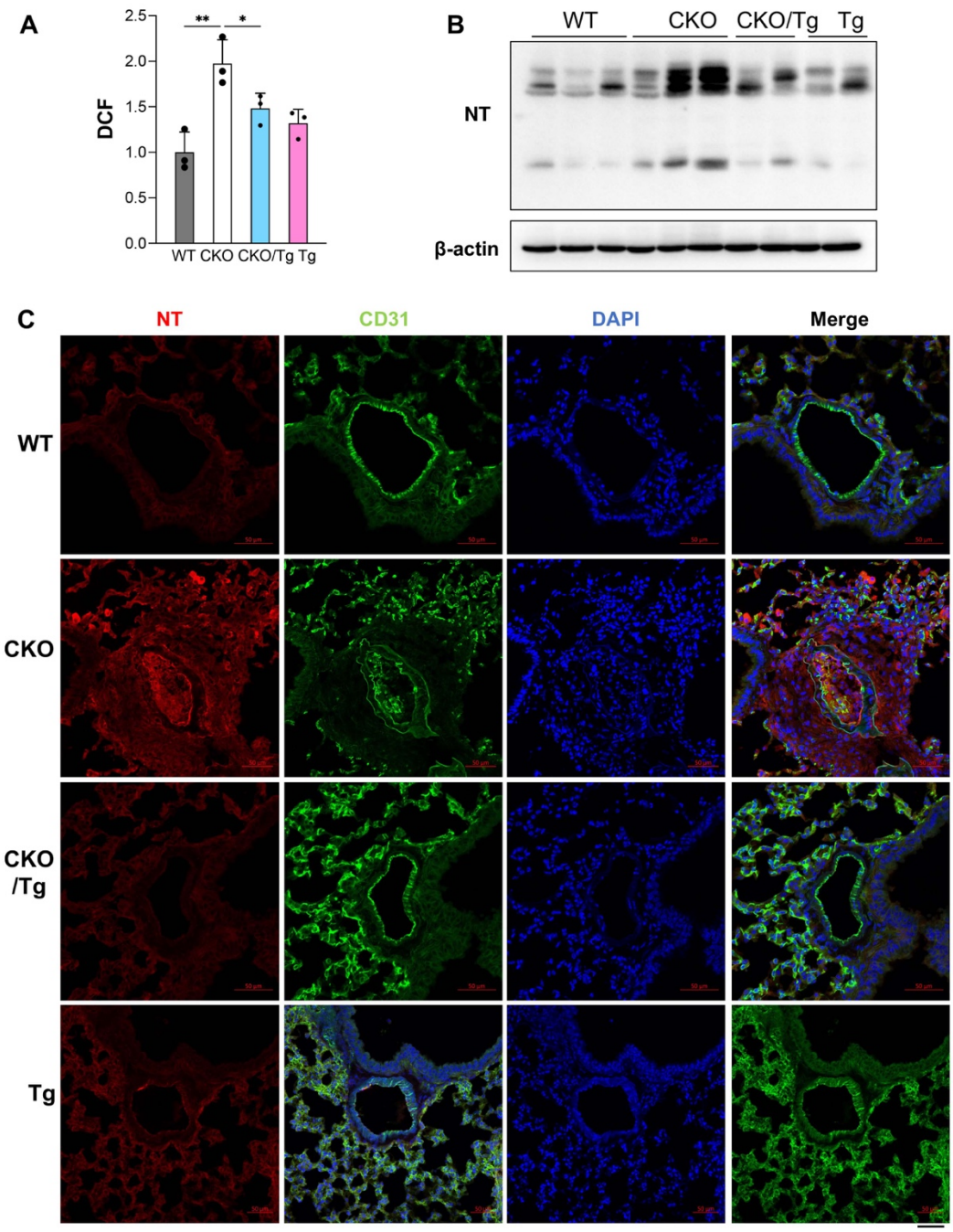


**Figure 6. Endothelial Cav1 transgenic expression inhibited excessive ROS/RNS in *Egln1*$^{Tie2Cre}$ mouse lungs.** (**A**) DCF measurements demonstrating the increased production of ROS/RNS seen in *Egln1*$^{Tie2Cre}$ (CKO) mouse lungs was inhibited in *CKO/Tg* mouse lungs. There is no marked difference in lung generation of ROS/RNS in *Cav1*$^{EC\text{-}Tg}$ (Cav1Tg) mice compared to WT mice. WT and CKO data shared with **Fig. 1A**. (**B**) Western Blotting demonstrated the reduction of NT levels in *CKO/Tg* mice compared to *Egln1*$^{Tie2Cre}$ (CKO) mice. (**C**) Immunostaining showed that CKO/Tg mice

exhibited reduction of NT levels compared to CKO mice. Lung sections were immunostained with anti-NT (red) and CD31 (Green). Nuclei were counterstained with DAPI (blue). *, $P < 0.05$, **, $P < 0.01$. One-way ANOVA and Tukey post-hoc analysis (**A**).

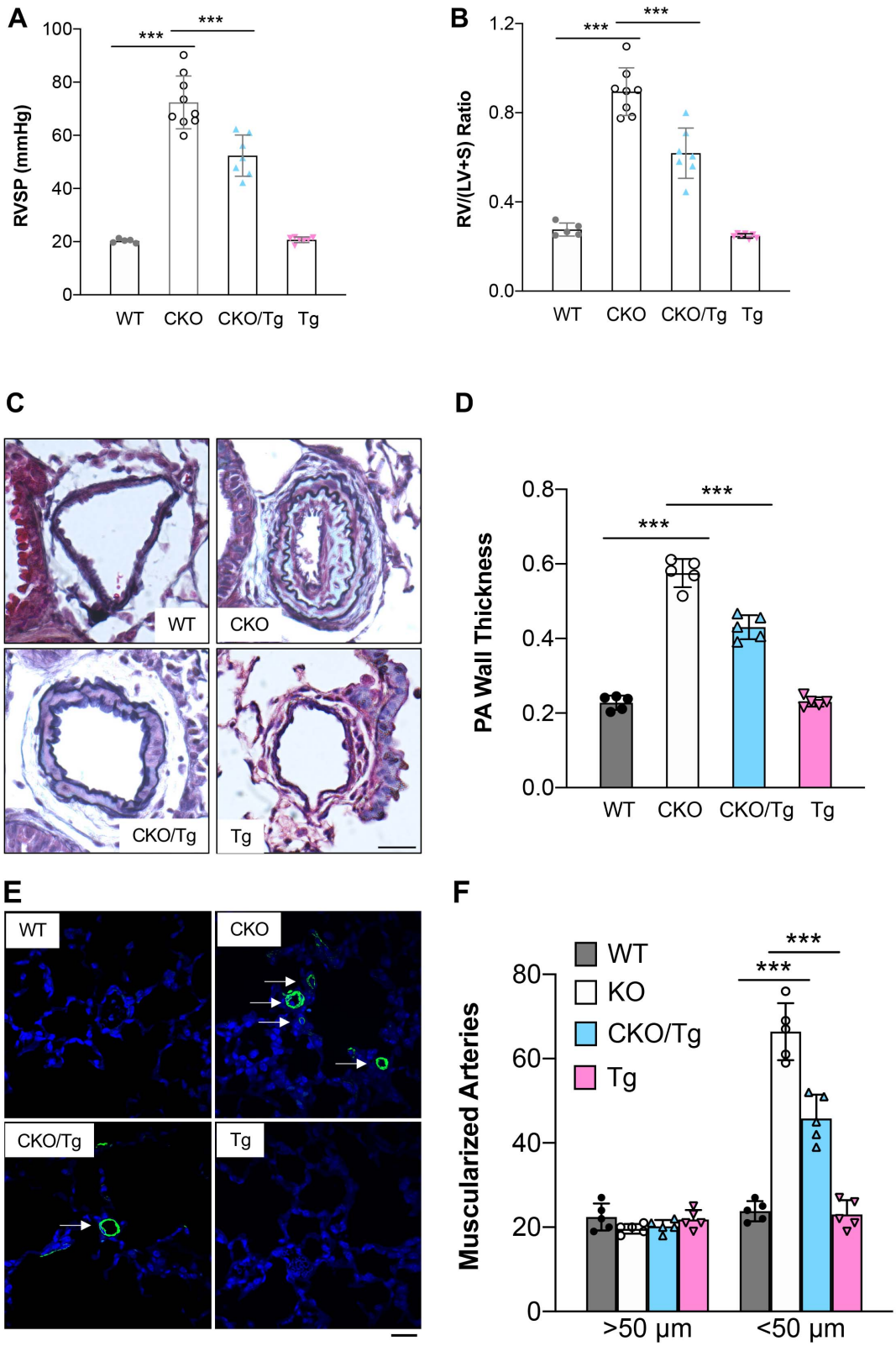


**Figure 7. Transgenic expression of Cav1 in ECs inhibited severe PAH seen in *Egln1$^{Tie2Cre}$* mice**. (**A**, **B**) *Egln1$^{Tie2Cre}$/Cav1$^{EC\text{-}Tg}$* (CKO/Tg) mice exhibited marked decreases of RVSP (**A**) and RV hypertrophy (**B**) compared to *Egln1$^{Tie2Cre}$* (CKO) mice

at age of 3.5-month old. (**C**, **D**) Representative micrographs of Pentachrome staining showing inhibited obliterative vascular remodeling including diminished neointima formation and reduced wall thickness in the lung of CKO/Tg mice. (**E**, **F**) Immunostaining of α-smooth muscle actin (α-SMA) demonstrating inhibition of muscularization of distal pulmonary vessels in the lungs of CKO/Tg mice. ***, $P<0.001$. One-way ANOVA and Tukey post-hoc analysis (**A**, **B**, **D** and **F**). Scale bar: 50μm.

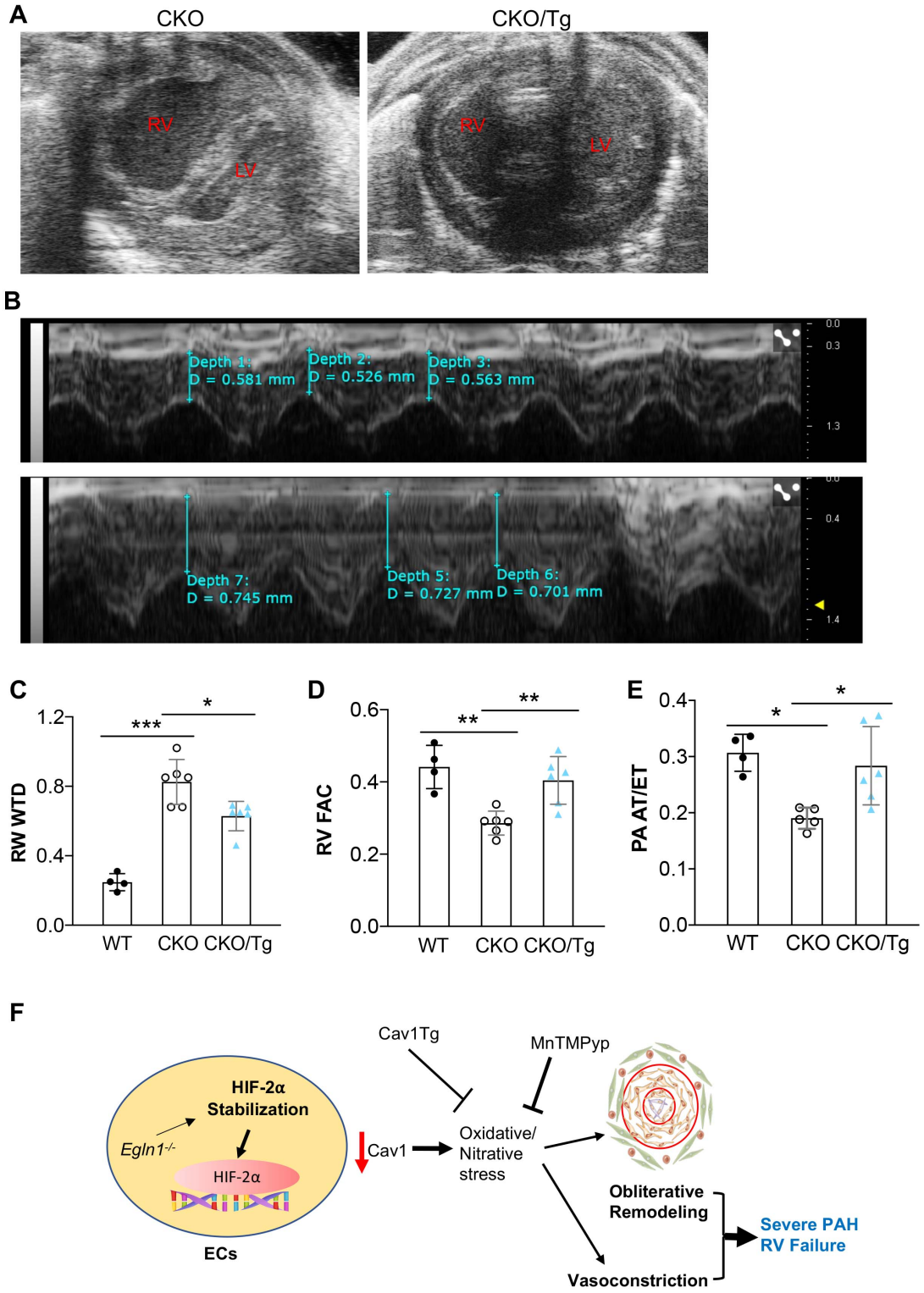


**Figure 8. Cav1 transgenic expression in ECs improved right heart function in** *Egln1*$^{Tie2Cre}$/ Cav1$^{EC\text{-}Tg}$ mice**.** (**A**) Representative echocardiography B-mode showing reduced RV chamber size in *Egln1*$^{Tie2Cre}$/ Cav1$^{EC\text{-}Tg}$ (CKO/Tg) mice compared to *Egln1*$^{Tie2Cre}$ mice. (**B**) Representative echocardiography M-mode showing reduced RV

wall thickness at diastolic stage in *Egln1*$^{Tie2Cre}$/ Cav1$^{EC\text{-}Tg}$ (CKO/Tg) mice compared to *Egln1*$^{Tie2Cre}$ mice. (**C**) RV wall thickening seen in *Egln1*$^{Tie2Cre}$ mice was inhibited in CKO/Tg mice. (**D**) RV contractility was improved by restored endothelial Cav1 expression in CKO/Tg mice compared to *Egln1*$^{Tie2Cre}$ mice. (**E**) Pulmonary arterial function assessed by PA AT/ET ratio was rescued in CKO/Tg mice. (**F**) A diagram showing that PHD2 deficiency induces decreases of endothelial Cav1 expression resulting in augmented nitrative stress which contributes to obliterative pulmonary vascular remodeling and severe PAH leading to RV failure. Restoration of endothelial Cav1 expression or ROS scavenging may be therapeutic approaches for the treatment of PAH. *, $P< 0.05$, **, $P<0.01$. One-way ANOVA and Tukey post-hoc analysis (**C-E**).

**Supplemental Figure legends**

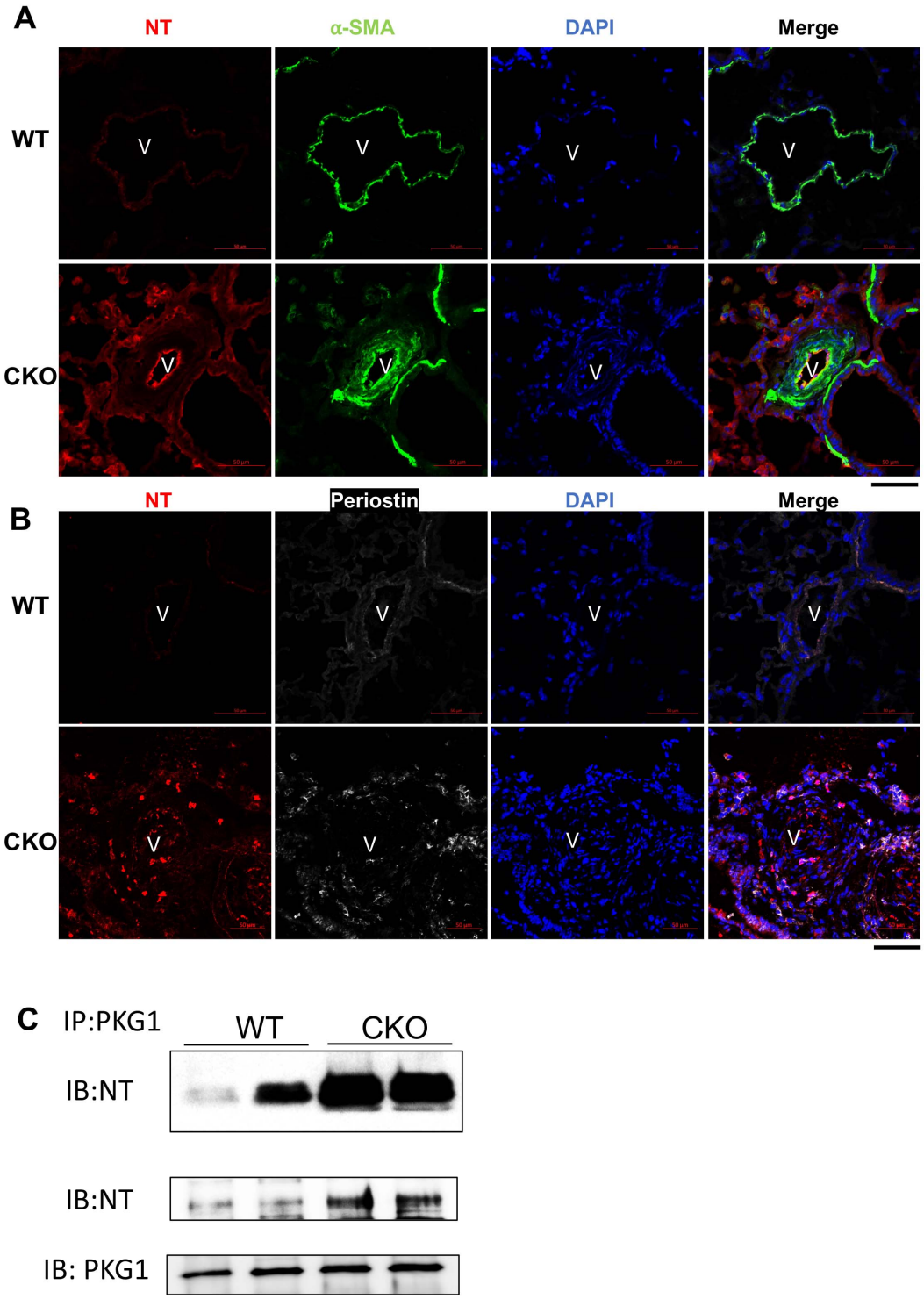


**Supplemental Figure 1. Upregulation of Nitrative stress in pulmonary vascular lesions in *Egln1*$^{Tie2Cre}$ mice. (A and B)** Representative micrographs of immunostaining showing relatively low levels of NT expression in pulmonary vascular lesions in

*Egln1*$^{Tie2Cre}$ mice (3.5 months old). Lung sections were immunostained with anti-NT antibody (red) for detection of nitrative stress. Anti- α-SMA antibodies were used to label smooth muscle cells (green, **A**). Anti-Periostin antibodies were used to label fibroblasts (white, **B**). Nuclei were counterstained with DAPI (blue). (**C**) Immunoprecipitation assay demonstrated that PKG nitrotyrosine modification was increased in CKO mice. Lung homogenates lysates were immunoprecipitated by PKG antibodies and blotted with anti-NT antibodies.

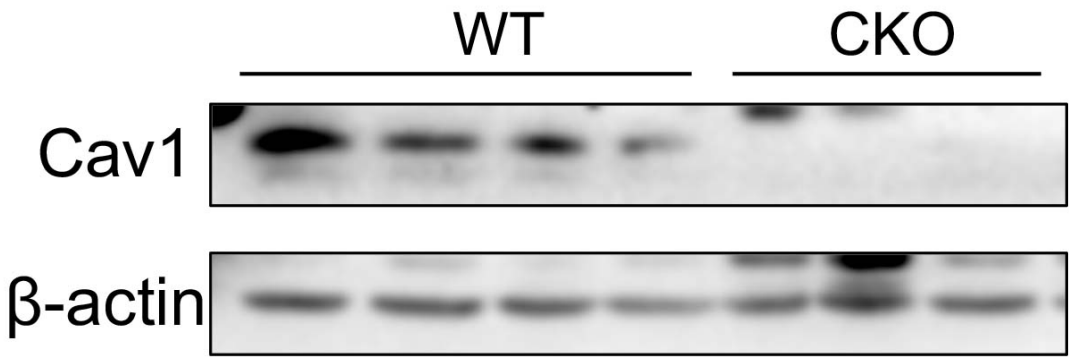


**Supplemental Figure 2. Cav1 expression is deficient in the lung of *Egln1*$^{Tie2Cre}$ mice. (A)** Western Blotting showing the downregulation of Cav1 expression in the lung of *Egln1*$^{Tie2Cre}$ mice compared to WT mice.

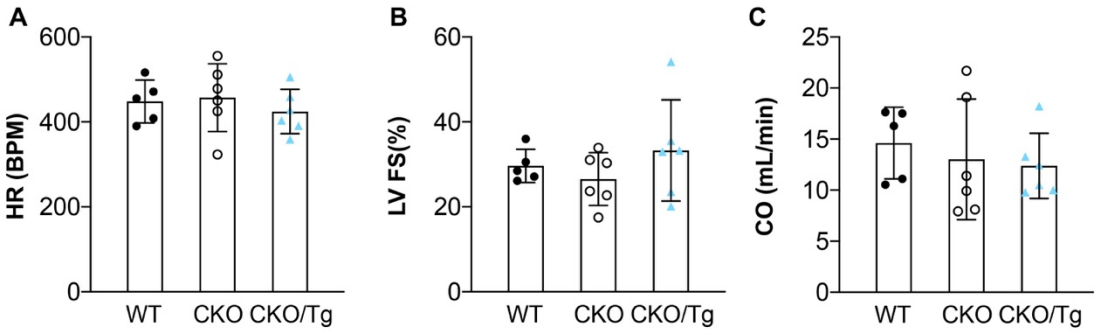


**Supplemental Figure 3. Cardiac size and function of CKO/Tg mice.** Heart rate (**A**), left ventricular fraction shorting (**B**), and cardiac output (**C**) were not changed in CKO/Tg mice compared to *Egln1*$^{Tie2Cre}$ mice. One-way ANOVA and Tukey post-hoc analysis (A-C).

**Supplemental Video 1, Echocardiography M-Mode of *Egln1*$^{Tie2Cre}$ (CKO) mice.**

DOI: 10.6084/m9.figshare.16674463

**Supplemental Video 2, Echocardiography M-Mode of *CKO/Tg* mice.**

DOI: 10.6084/m9.figshare.16674478

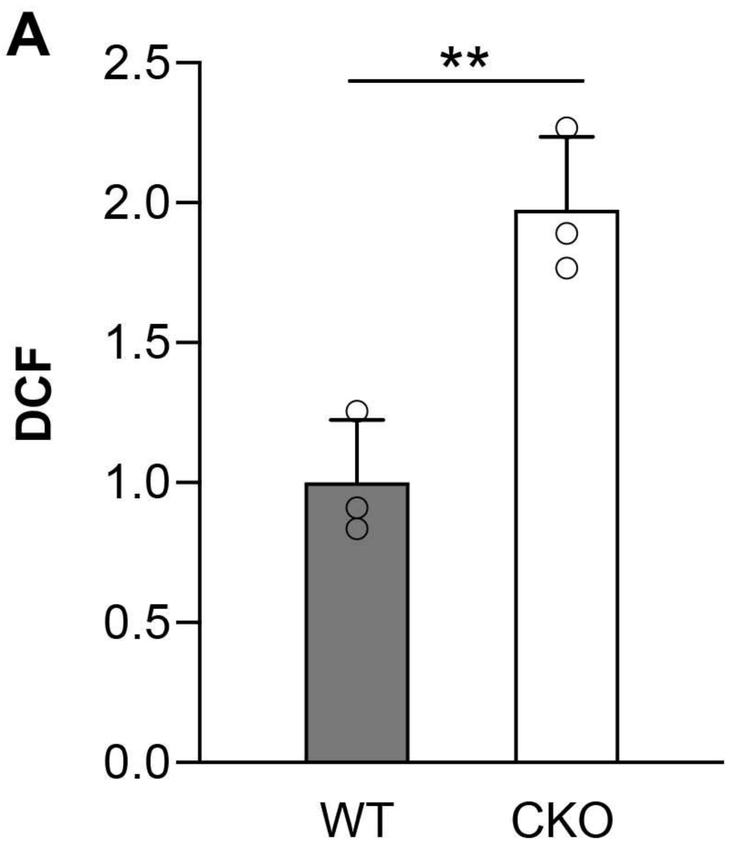
A
DCF
2.5
2.0
1.5
1.0
0.5
0.0
**
WT
CKO

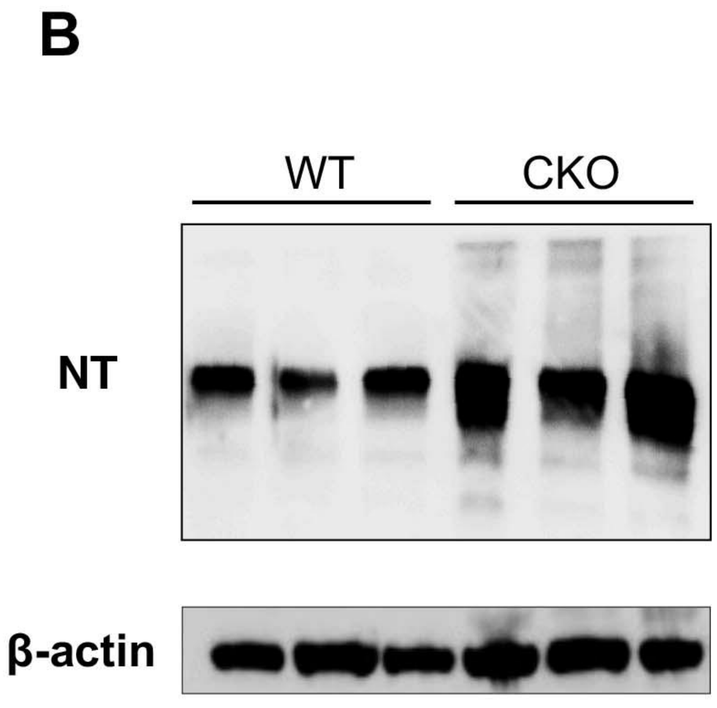
B
WT
CKO
NT
β-actin

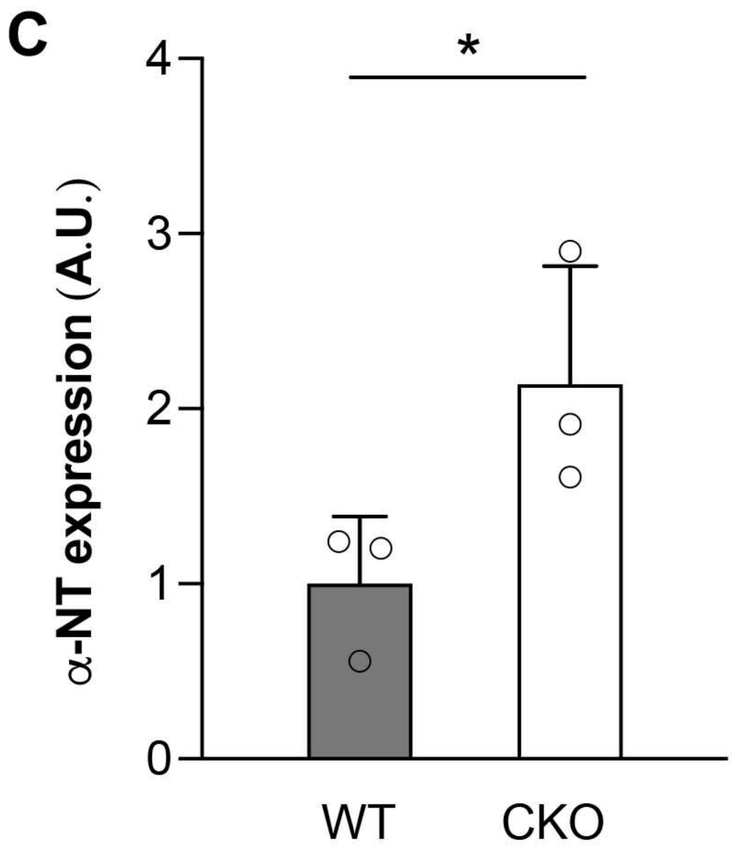
C
α-NT expression (A.U.)
4
3
2
1
0
*
WT
CKO

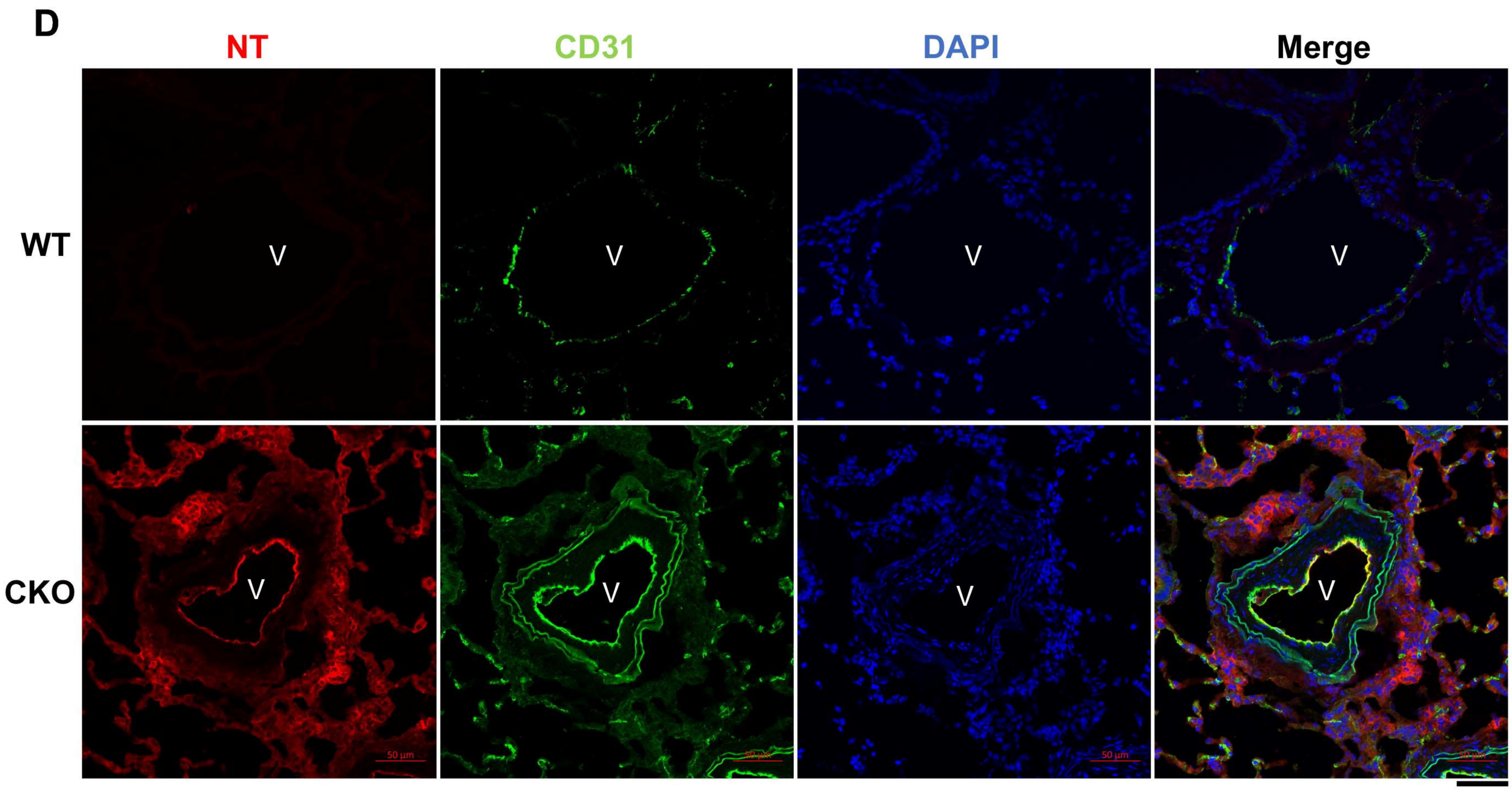
D
NT
CD31
DAPI
Merge
WT
CKO
V

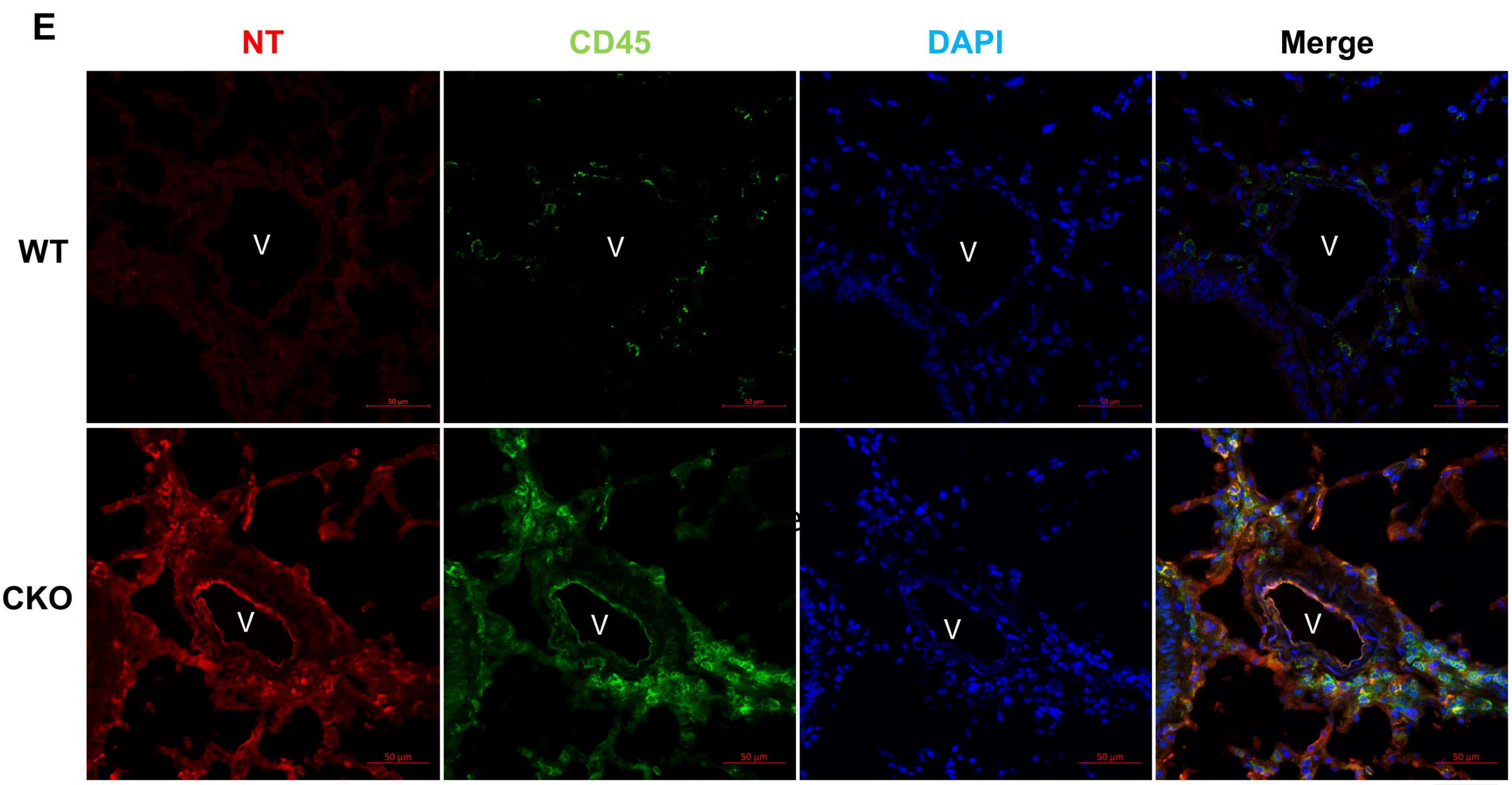
E
NT
CD45
DAPI
Merge
WT
CKO
V

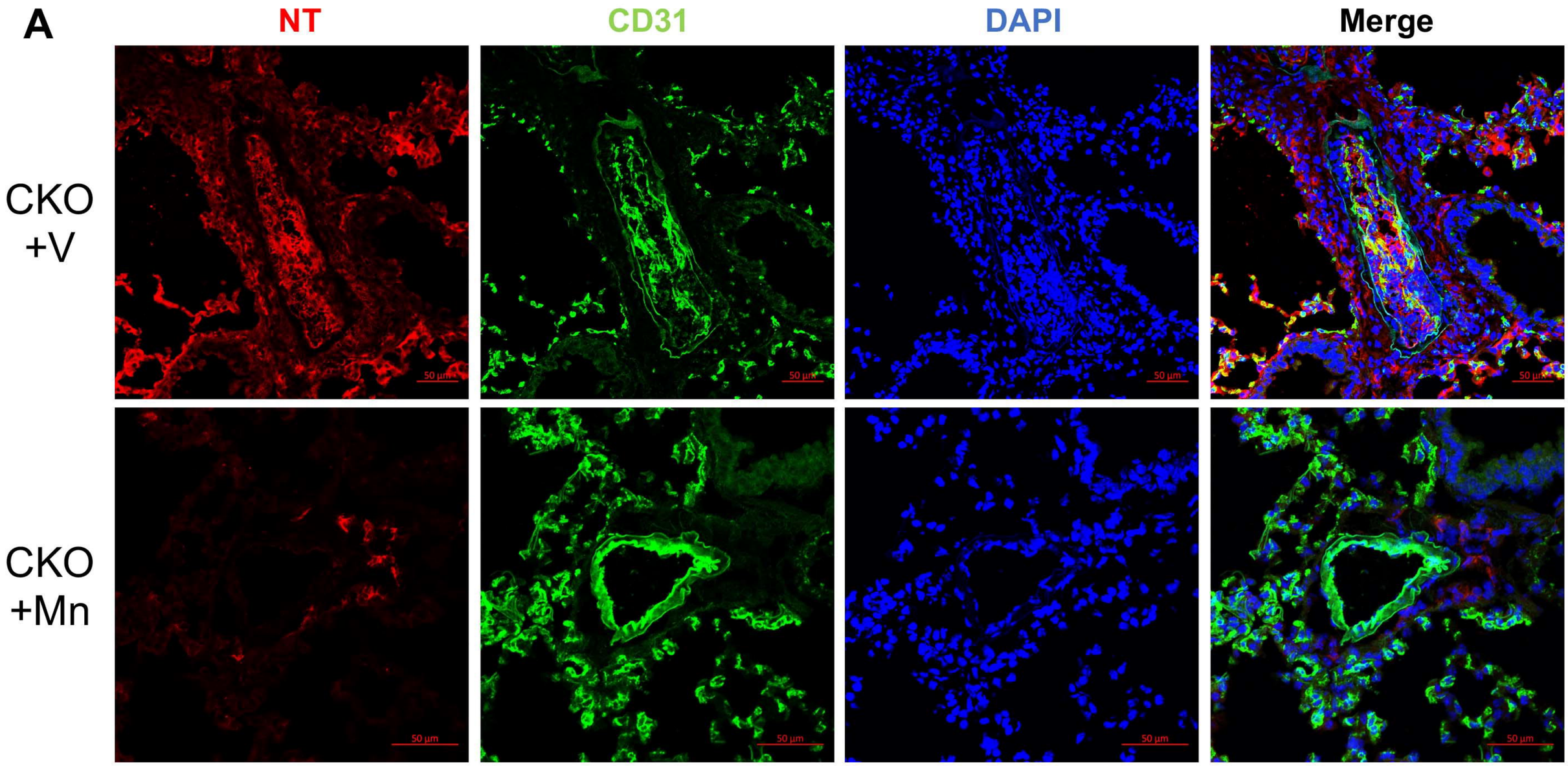
A
NT
CD31
DAPI
Merge
CKO +V
CKO +Mn
50 µm

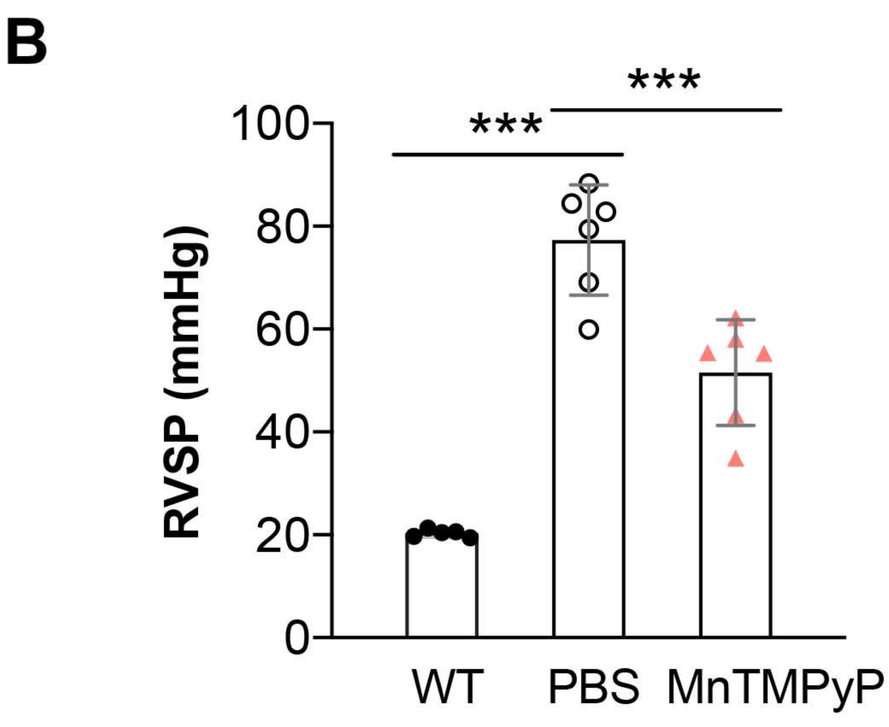
B
RVSP (mmHg)
100
80
60
40
20
0
***
***
WT
PBS
MnTMPyP

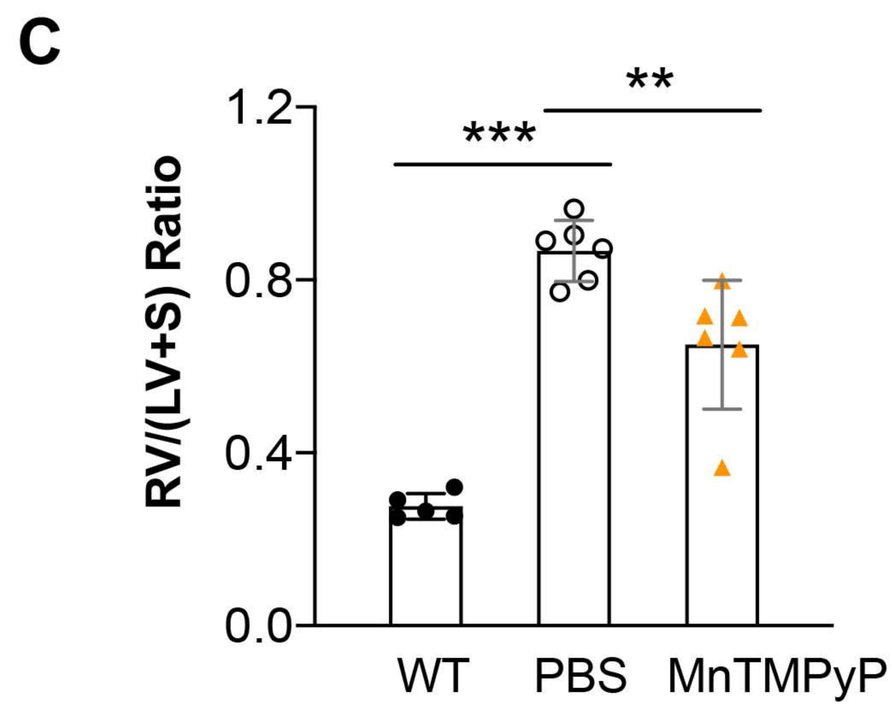
C
RV/(LV+S) Ratio
1.2
0.8
0.4
0.0
***
**
WT
PBS
MnTMPyP

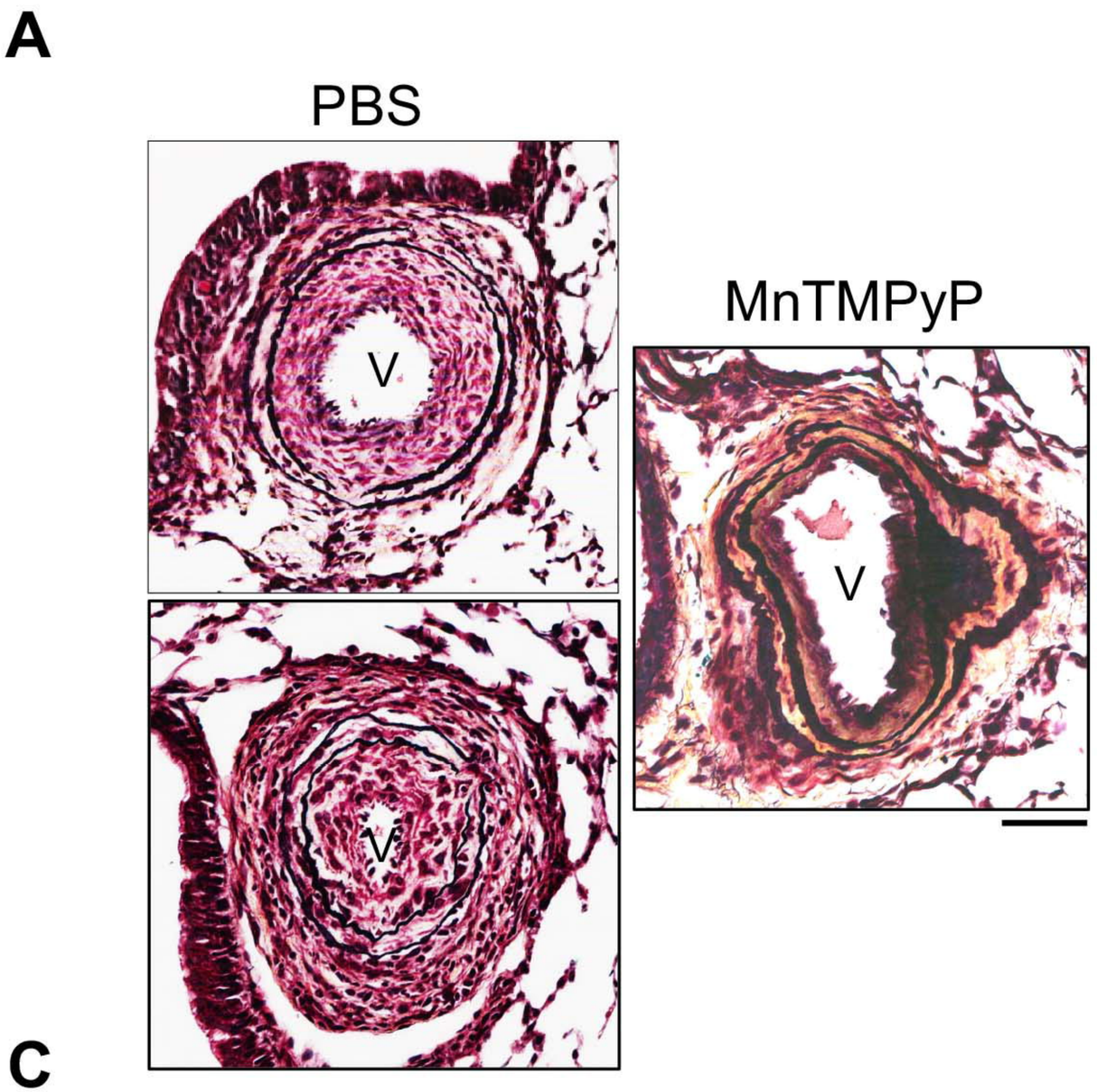
A
PBS
MnTMPyP
V
V
V

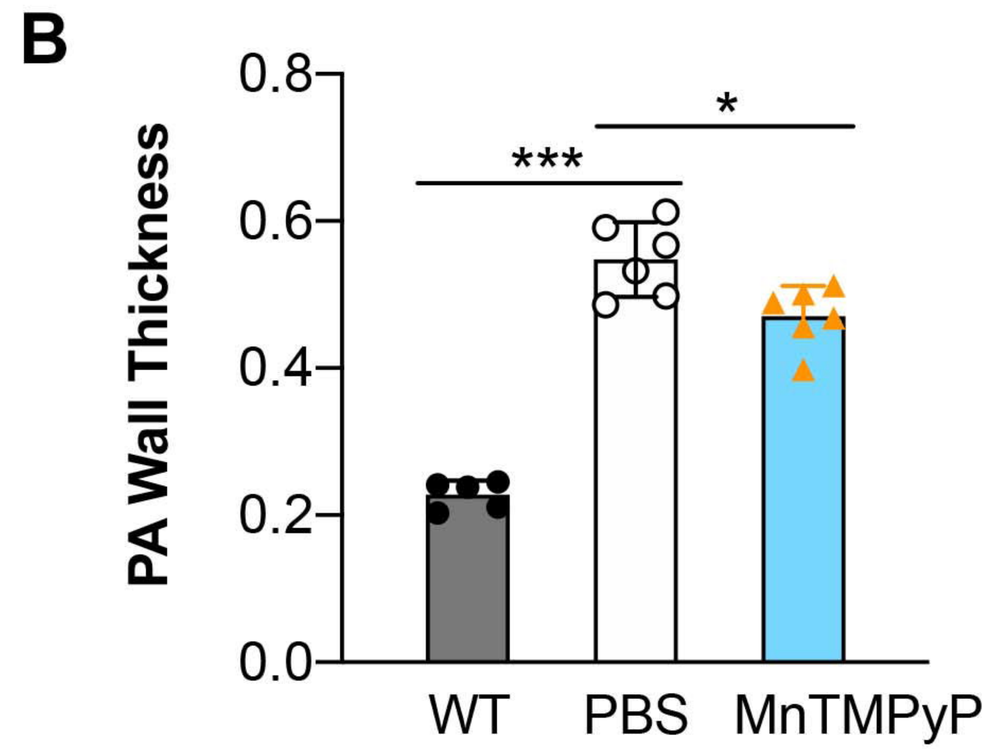
B
PA Wall Thickness
0.8
0.6
0.4
0.2
0.0
***
*
WT
PBS
MnTMPyP

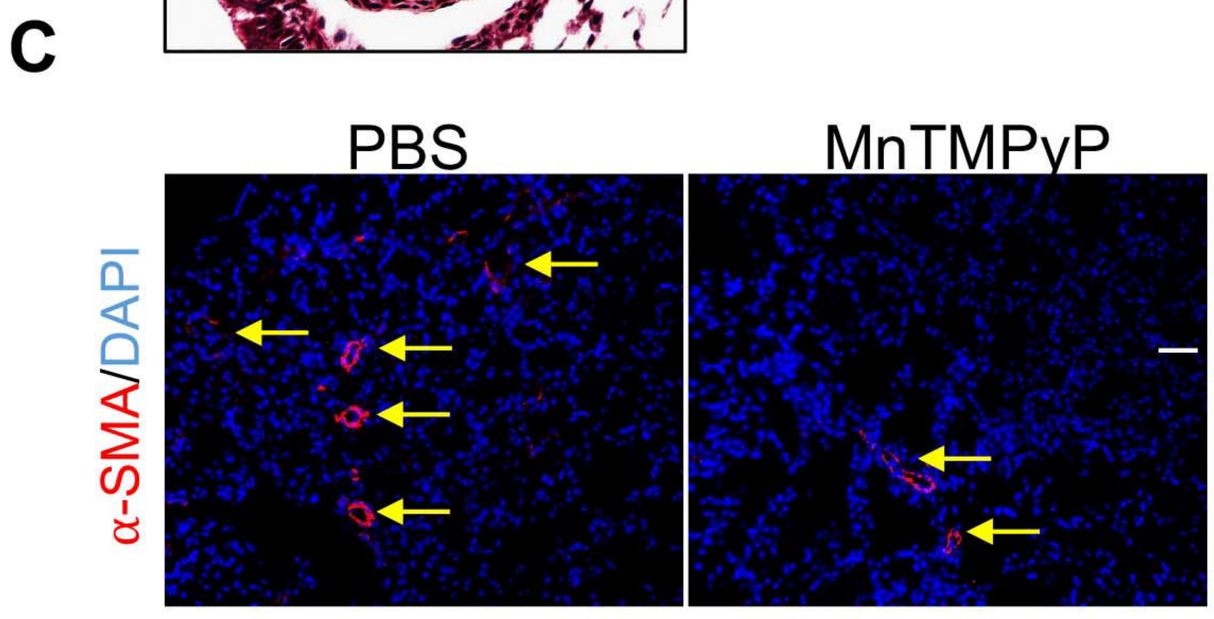
C
PBS
MnTMPyP
α-SMA/DAPI

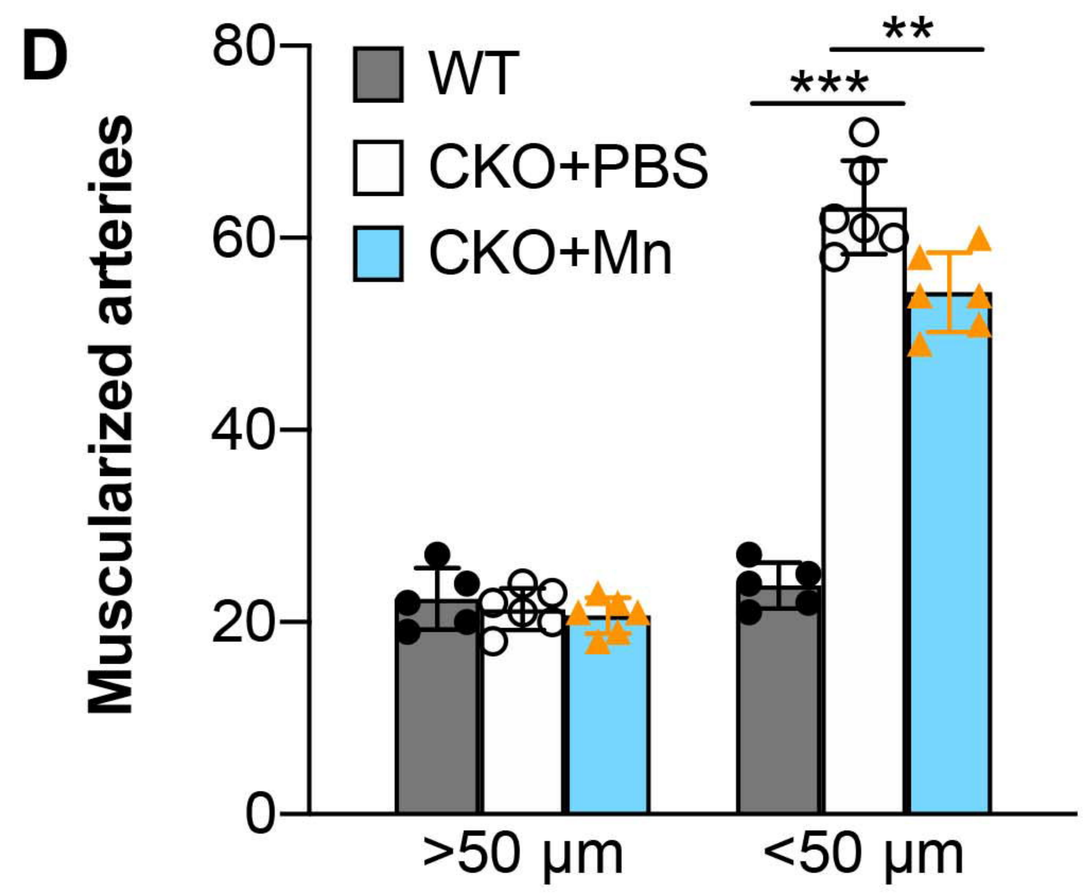
D
Muscularized arteries
80
60
40
20
0
WT
CKO+PBS
CKO+Mn
***
**
>50 μm
<50 μm

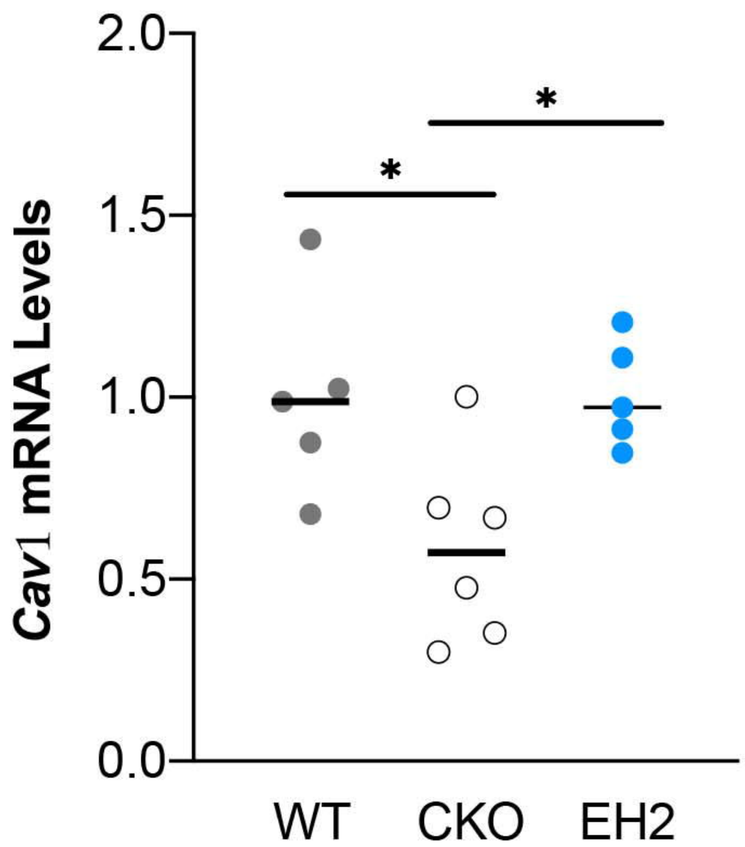
A
2.0
1.5
1.0
0.5
0.0
Cav1 mRNA Levels
*
*
WT
CKO
EH2

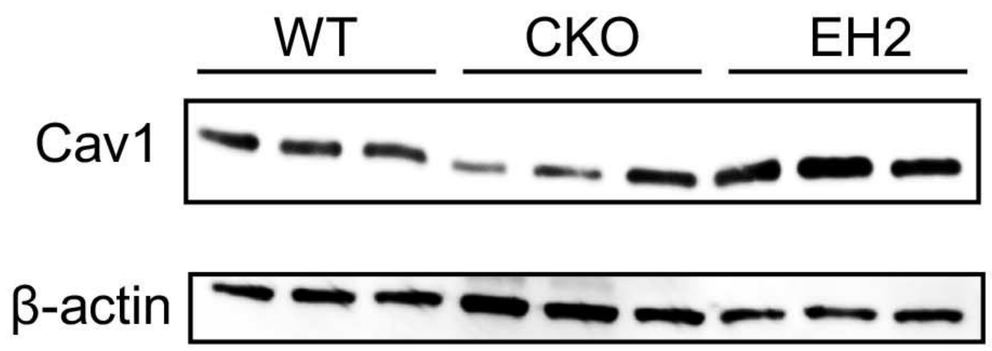
B
WT
CKO
EH2
Cav1
β-actin

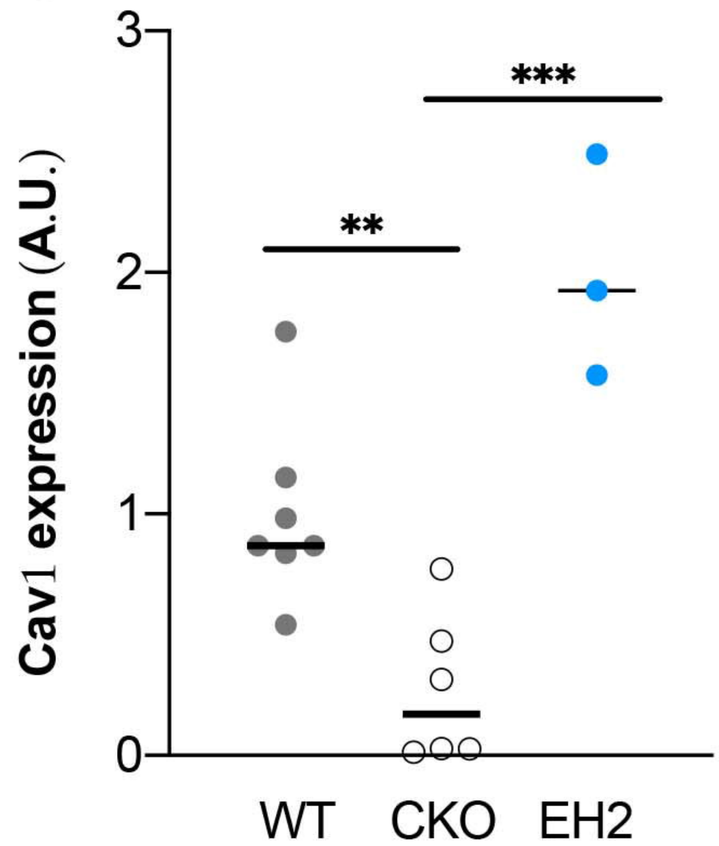
C
3
2
1
0
Cav1 expression (A.U.)
**
***
WT
CKO
EH2

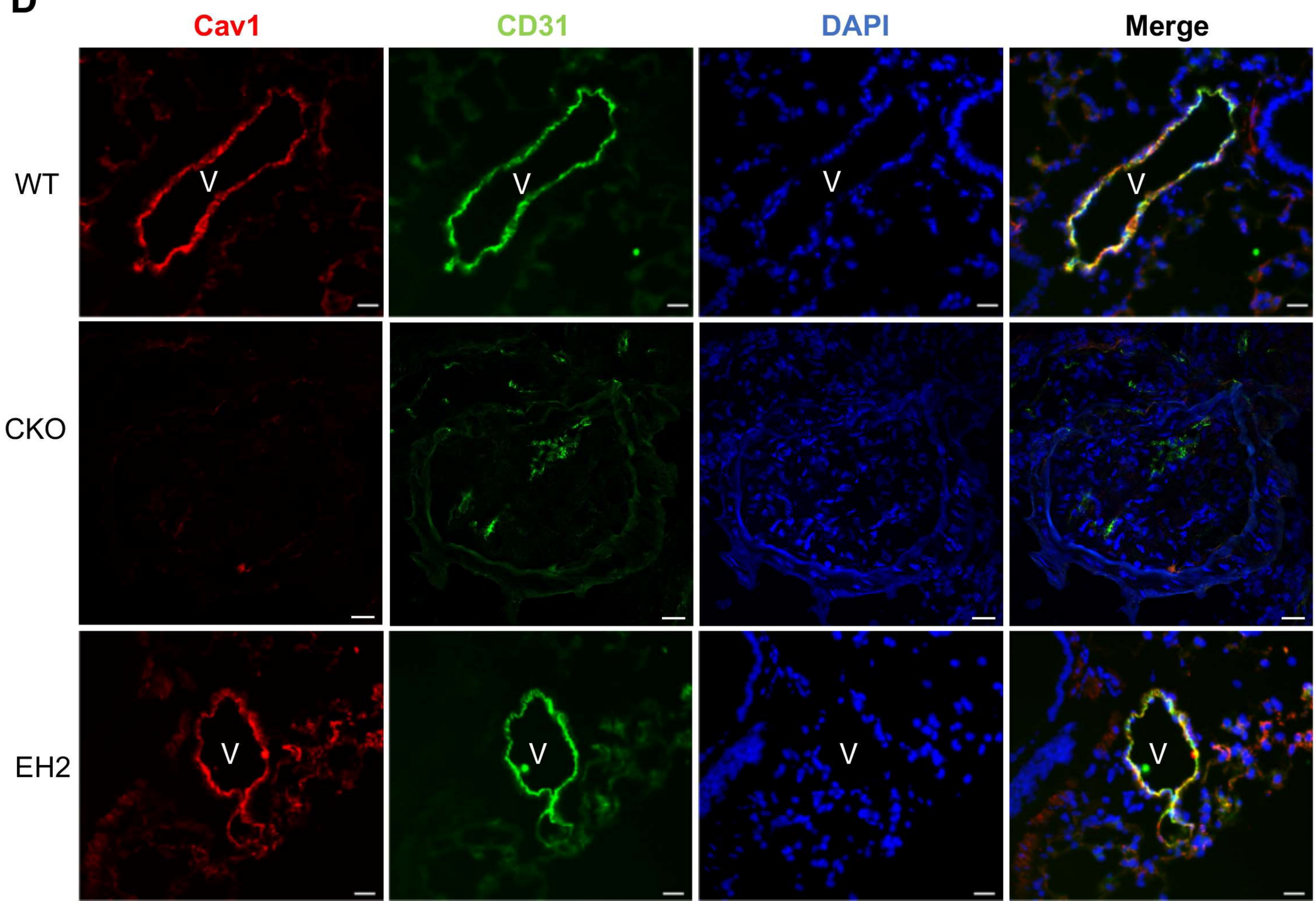
D
Cav1
CD31
DAPI
Merge
WT
CKO
EH2
V

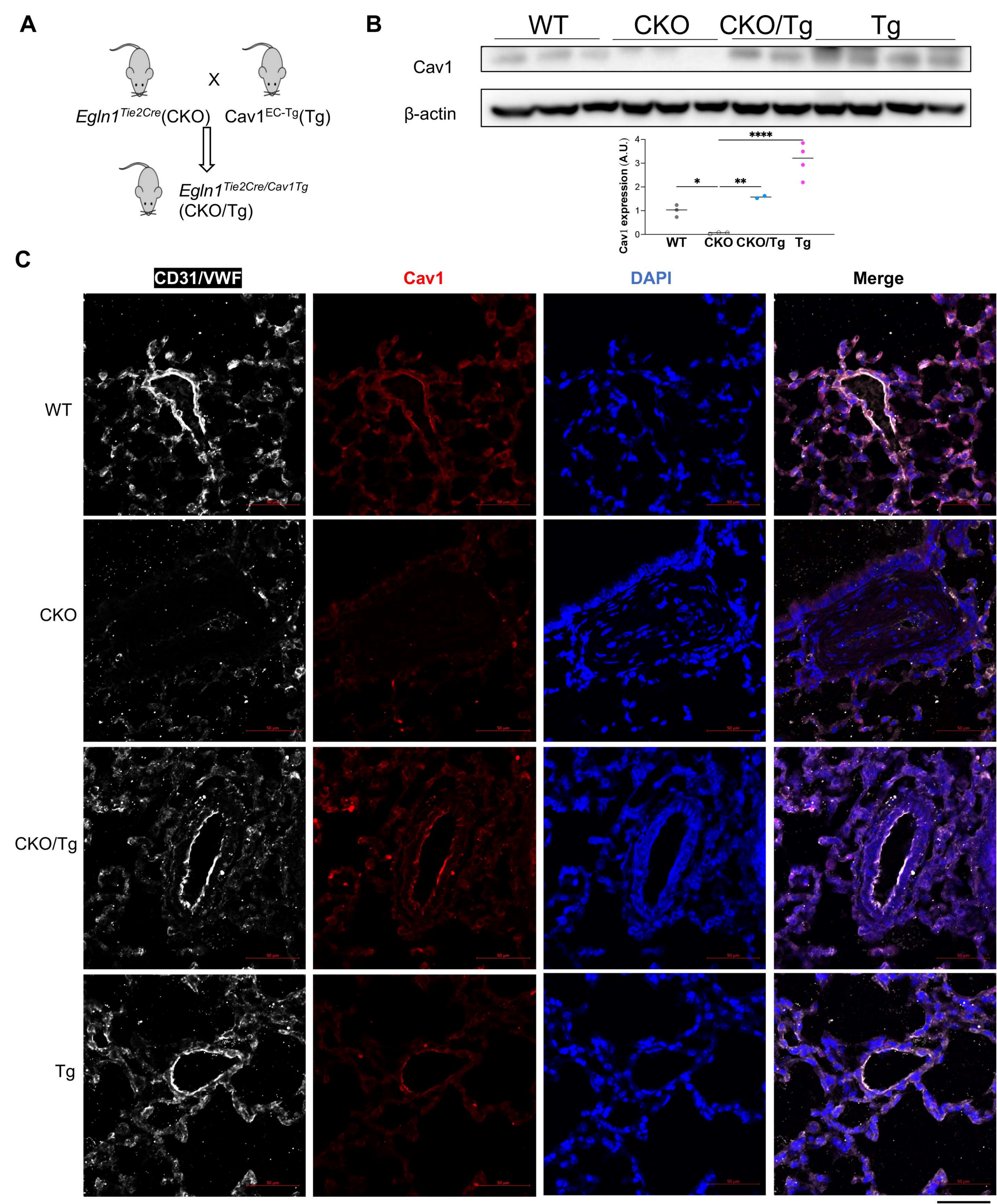
A
X
Egln1Tie2Cre(CKO)
Cav1EC-Tg(Tg)
Egln1Tie2Cre/Cav1Tg
(CKO/Tg)
B
WT
CKO
CKO/Tg
Tg
Cav1
β-actin
Cav1 expression (A.U.)
0
1
2
3
4
*
**
****
WT
CKO
CKO/Tg
Tg
C
CD31/VWF
Cav1
DAPI
Merge
WT
CKO
CKO/Tg
Tg
50 μm

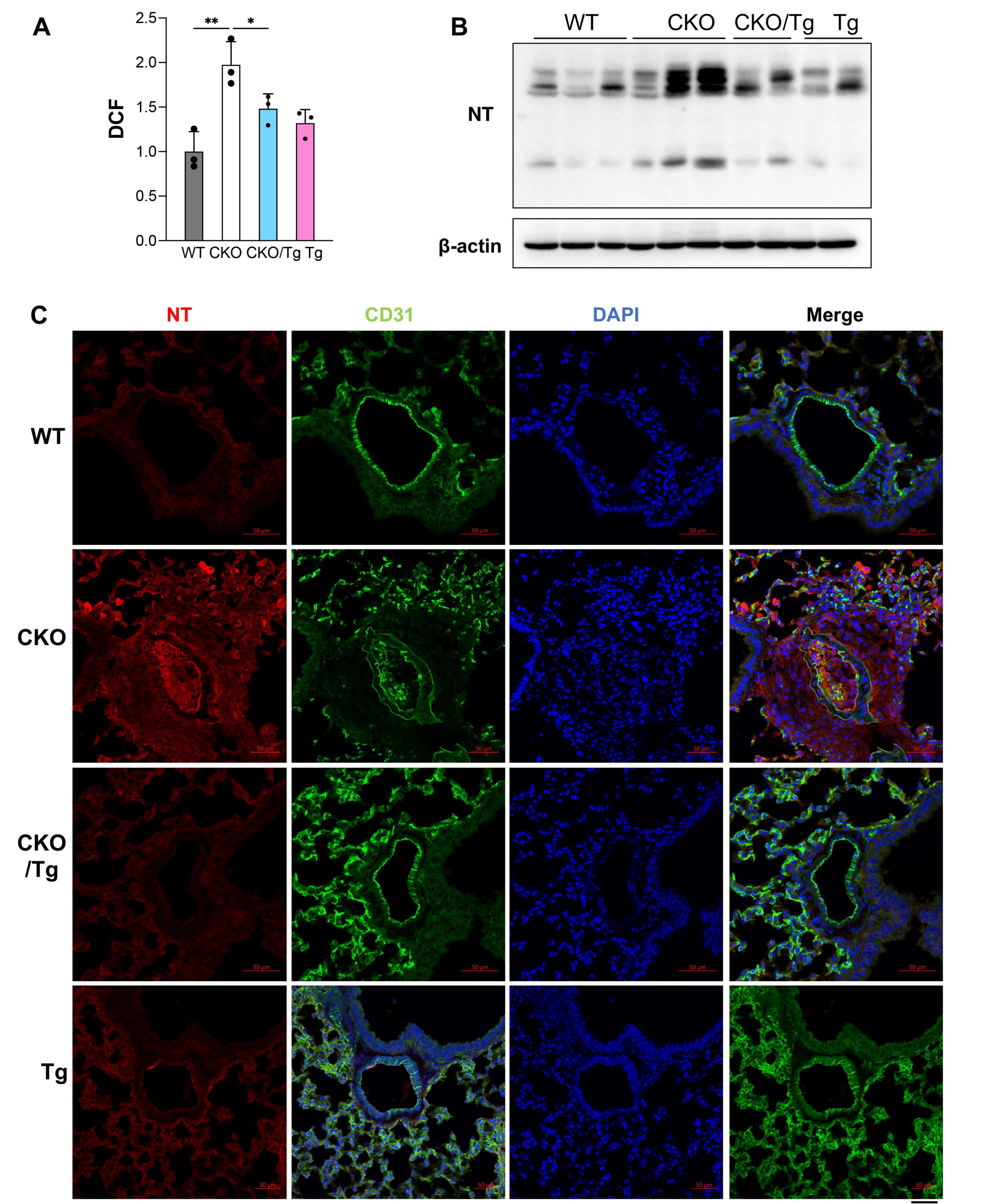
A
DCF
2.5
2.0
1.5
1.0
0.5
0.0
**
*
WT CKO CKO/Tg Tg
B
WT
CKO
CKO/Tg
Tg
NT
β-actin
C
NT
CD31
DAPI
Merge
WT
CKO
CKO /Tg
Tg
50 μm

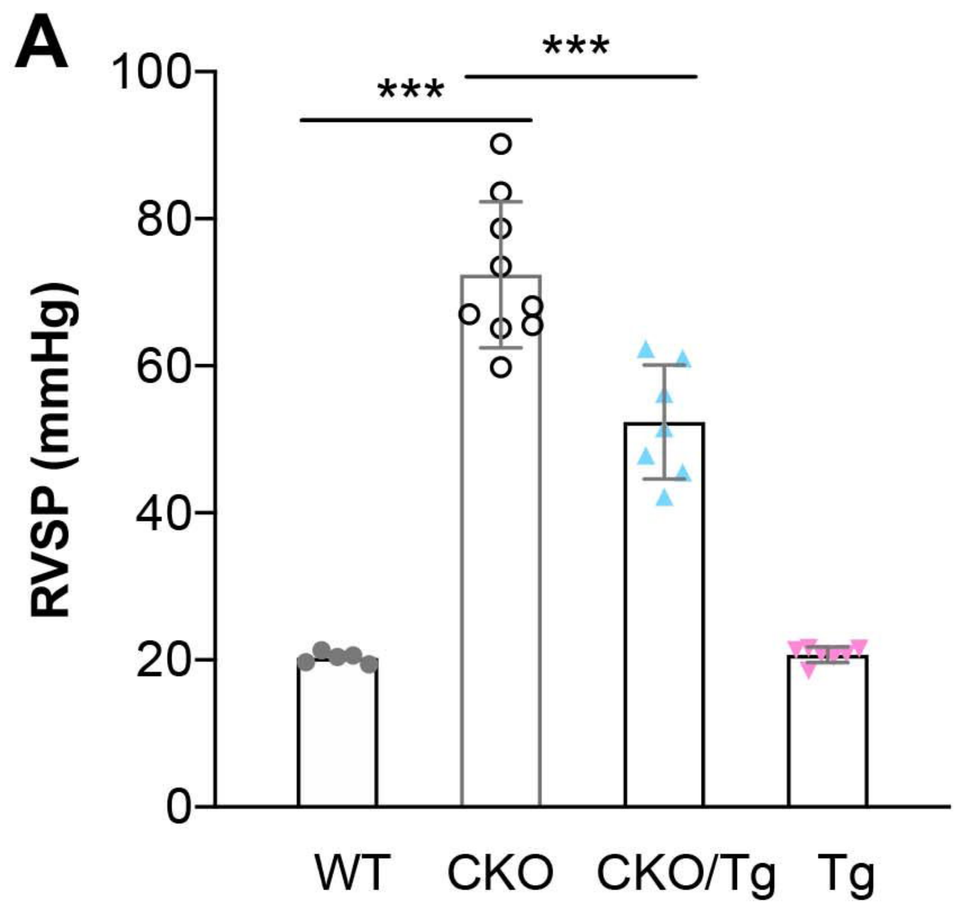
A
RVSP (mmHg)
100
80
60
40
20
0
***
***
WT
CKO
CKO/Tg
Tg

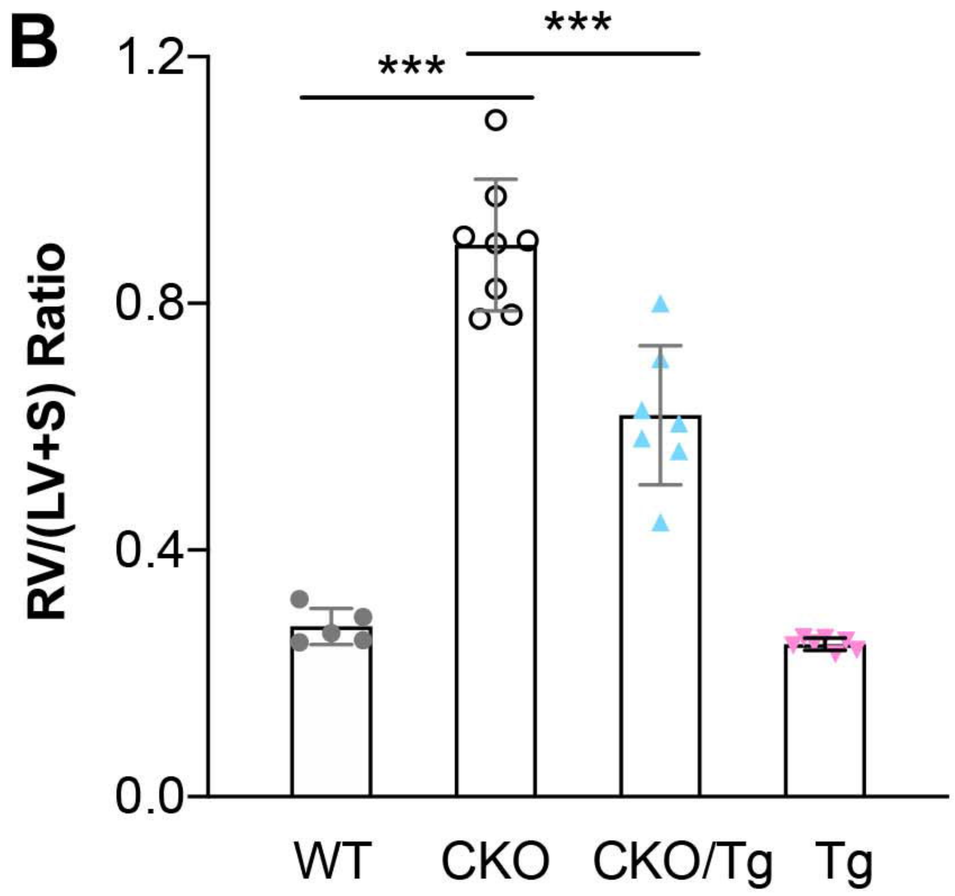
B
RV/(LV+S) Ratio
1.2
0.8
0.4
0.0
***
***
WT
CKO
CKO/Tg
Tg

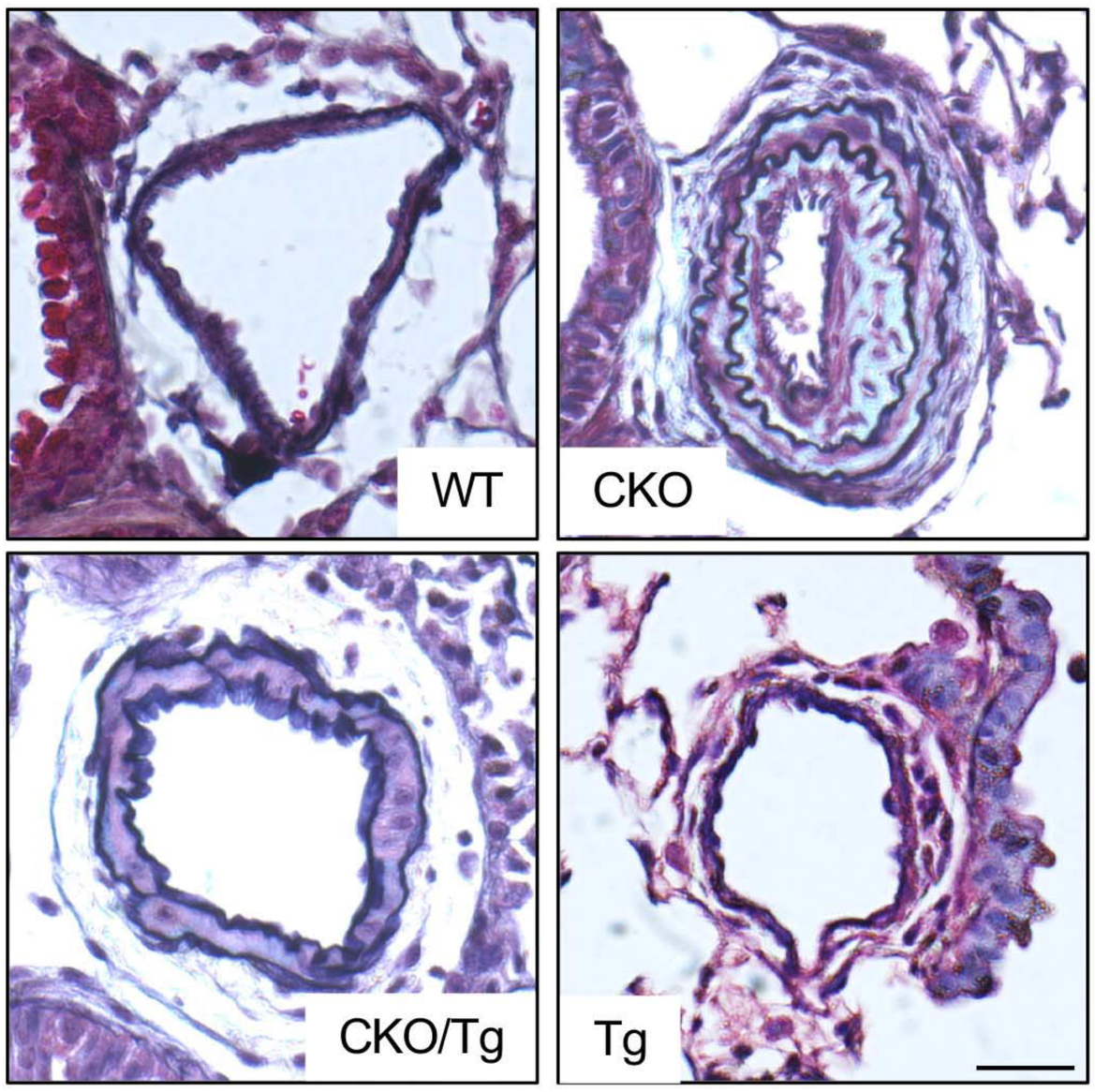
C
WT
CKO
CKO/Tg
Tg

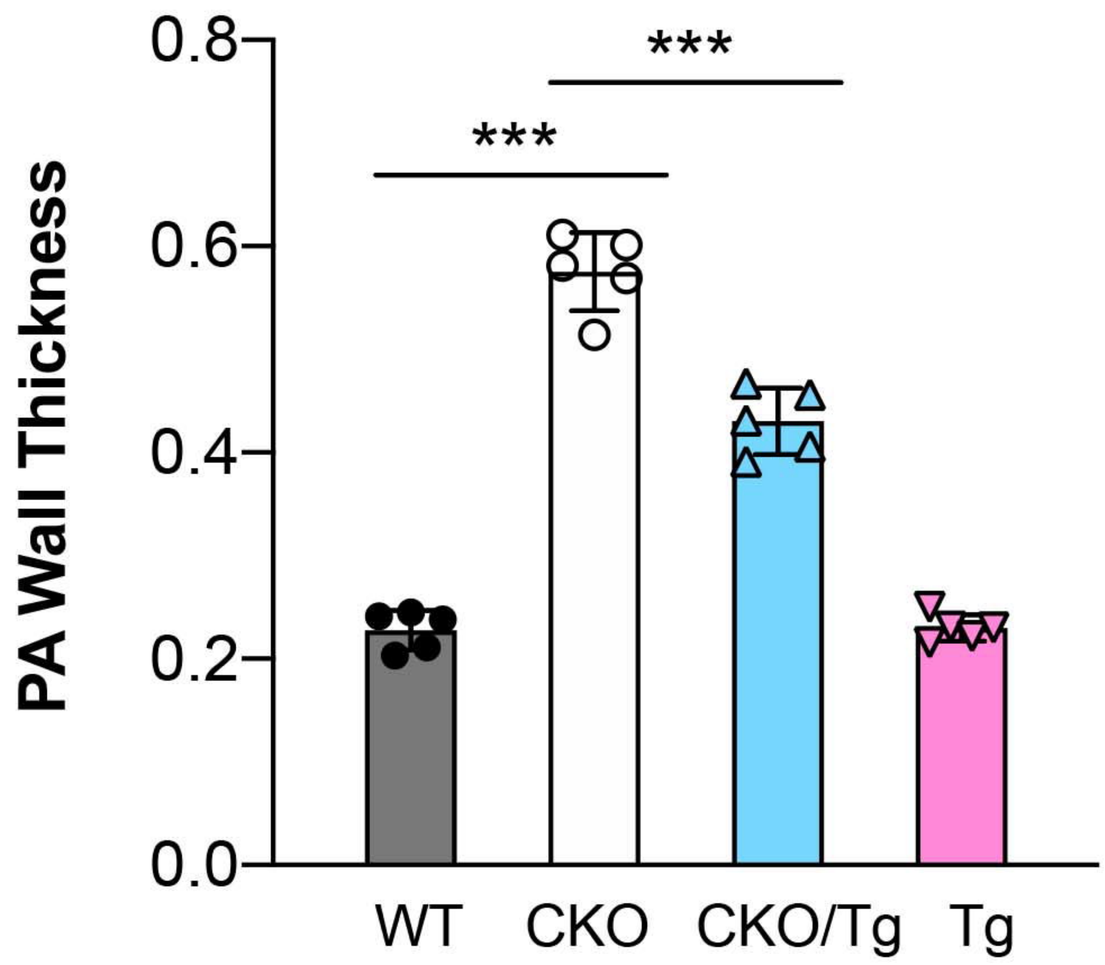
D
PA Wall Thickness
0.8
0.6
0.4
0.2
0.0
***
***
WT
CKO
CKO/Tg
Tg

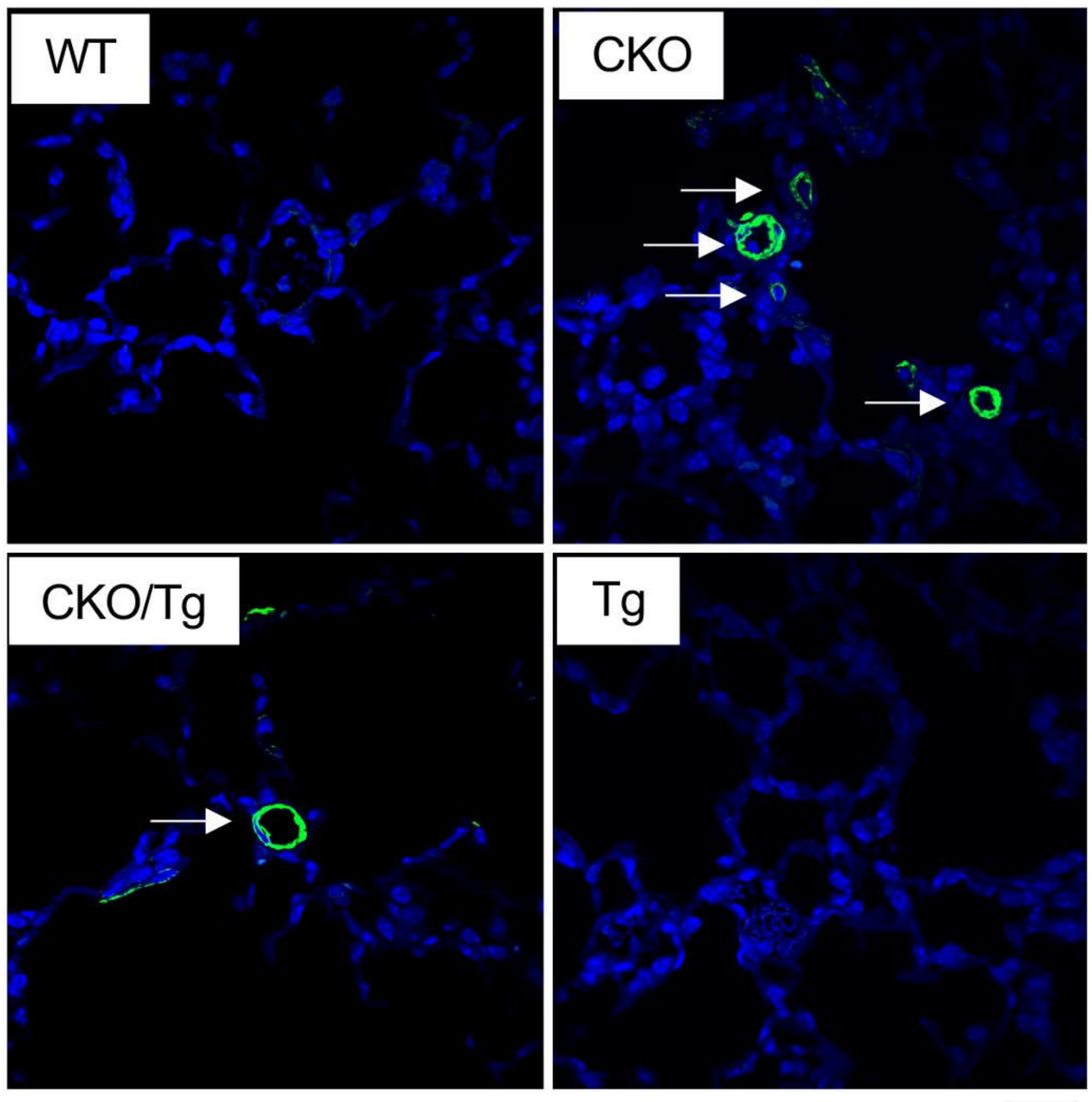
E
WT
CKO
CKO/Tg
Tg

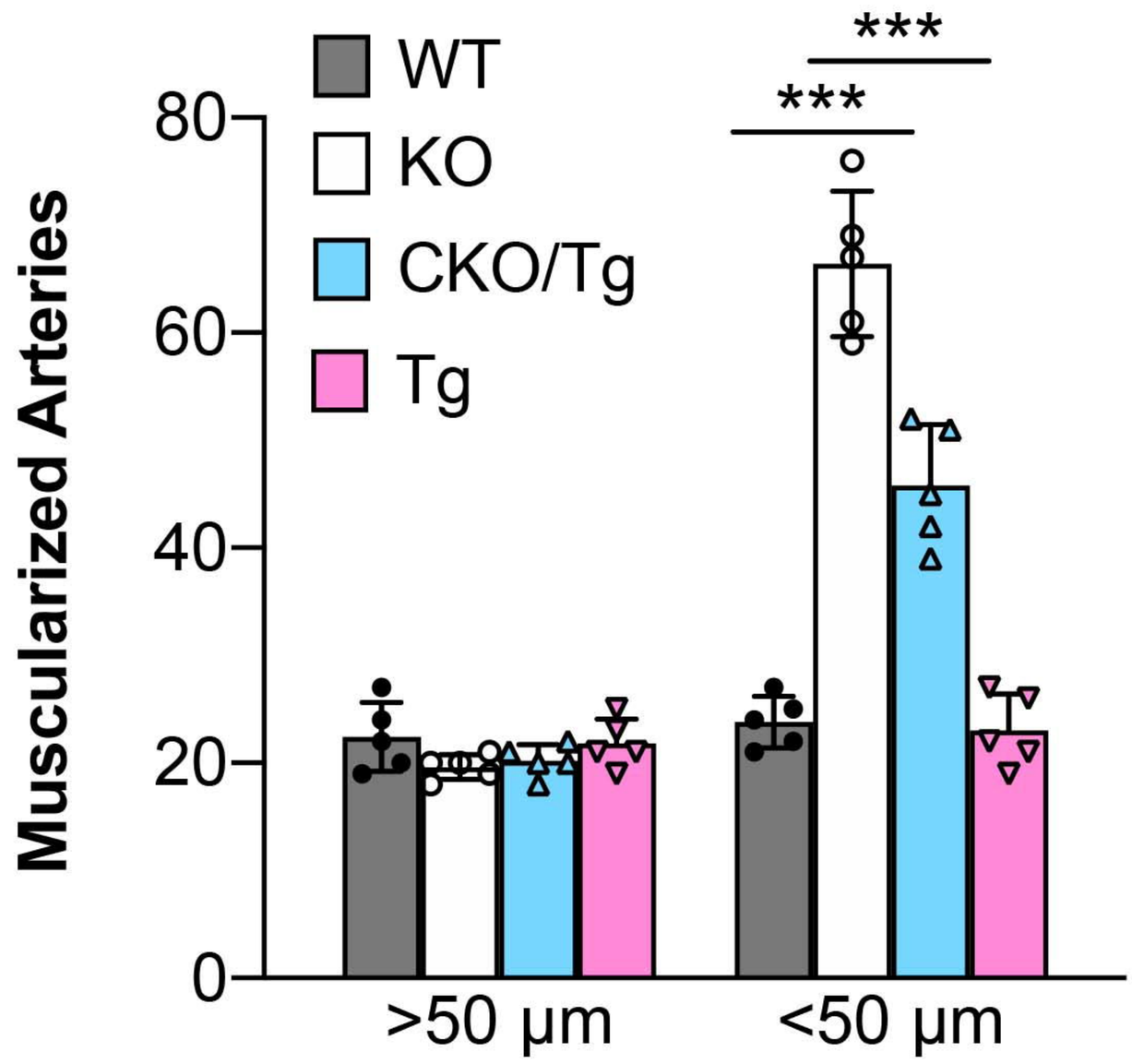
F
Muscularized Arteries
80
60
40
20
0
WT
KO
CKO/Tg
Tg
***
***
>50 µm
<50 µm

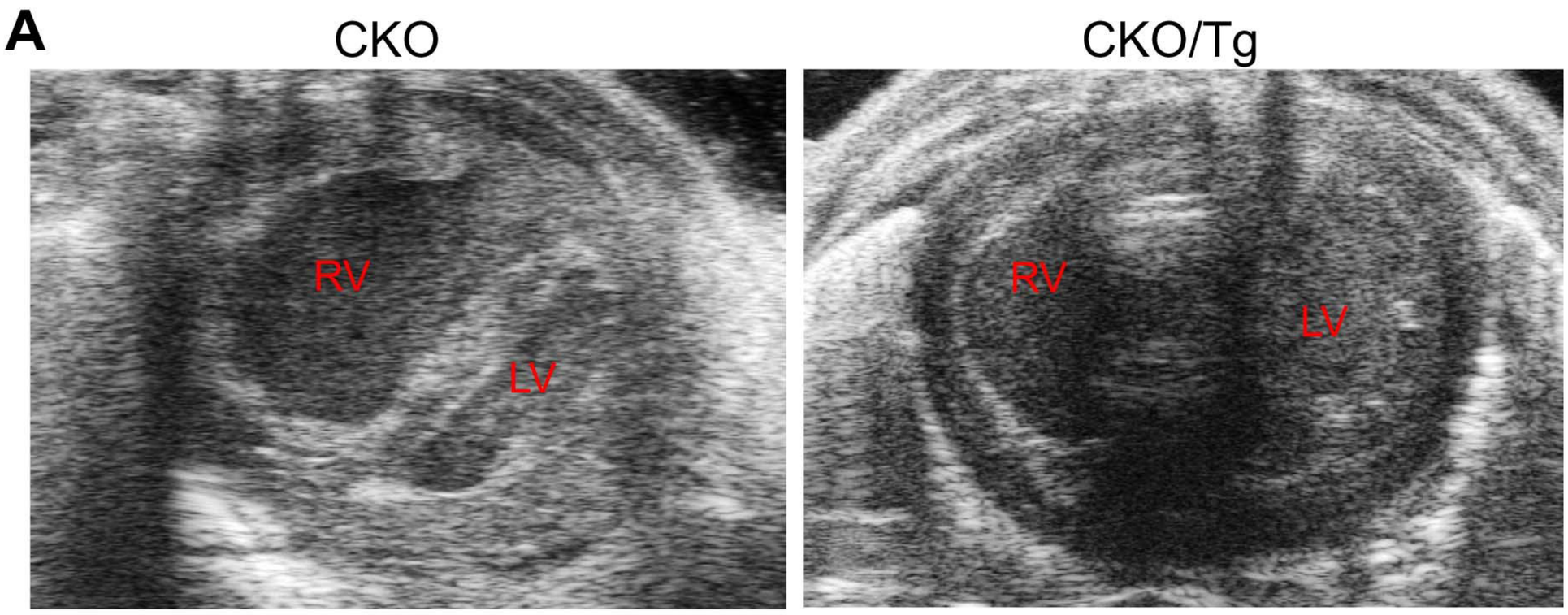
A
CKO
CKO/Tg
RV
LV
RV
LV

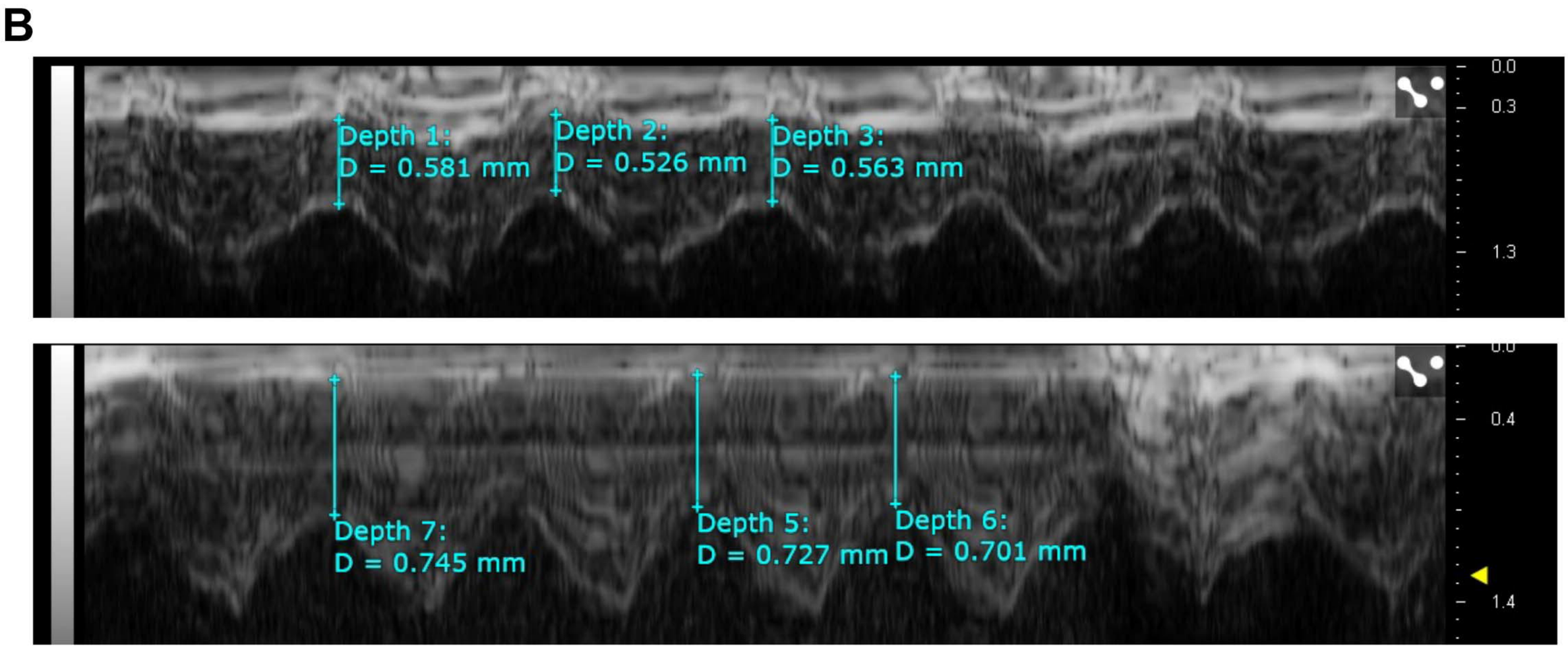
B
Depth 1:
D = 0.581 mm
Depth 2:
D = 0.526 mm
Depth 3:
D = 0.563 mm
0.0
0.3
1.3
Depth 7:
D = 0.745 mm
Depth 5:
D = 0.727 mm
Depth 6:
D = 0.701 mm
0.4
1.4

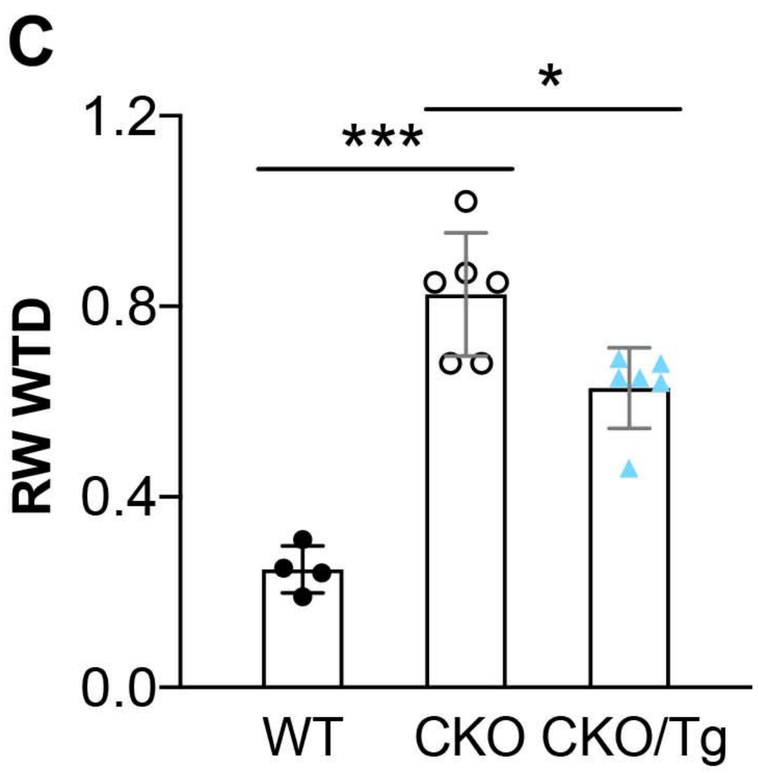
C
RW WTD
1.2
0.8
0.4
0.0
***
*
WT
CKO
CKO/Tg

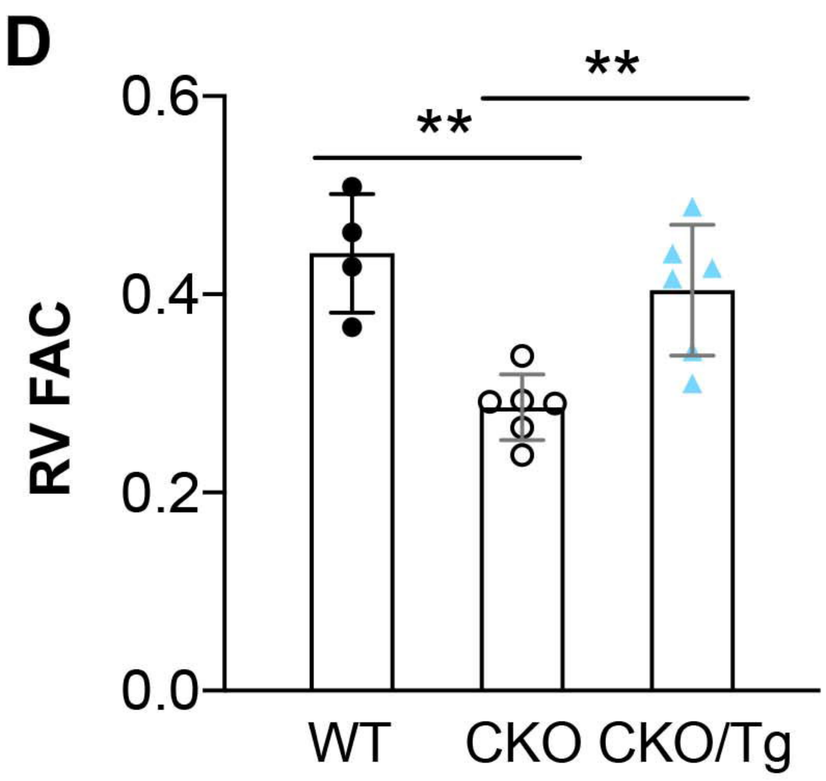
D
RV FAC
0.6
0.4
0.2
0.0
**
**
WT
CKO
CKO/Tg

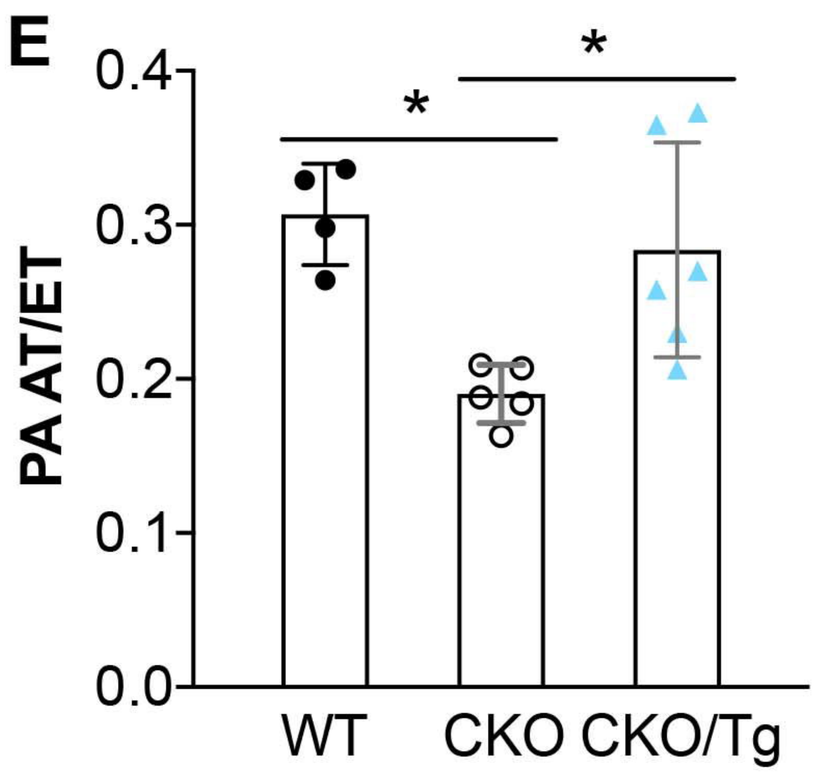
E
PA AT/ET
0.4
0.3
0.2
0.1
0.0
*
*
WT
CKO
CKO/Tg

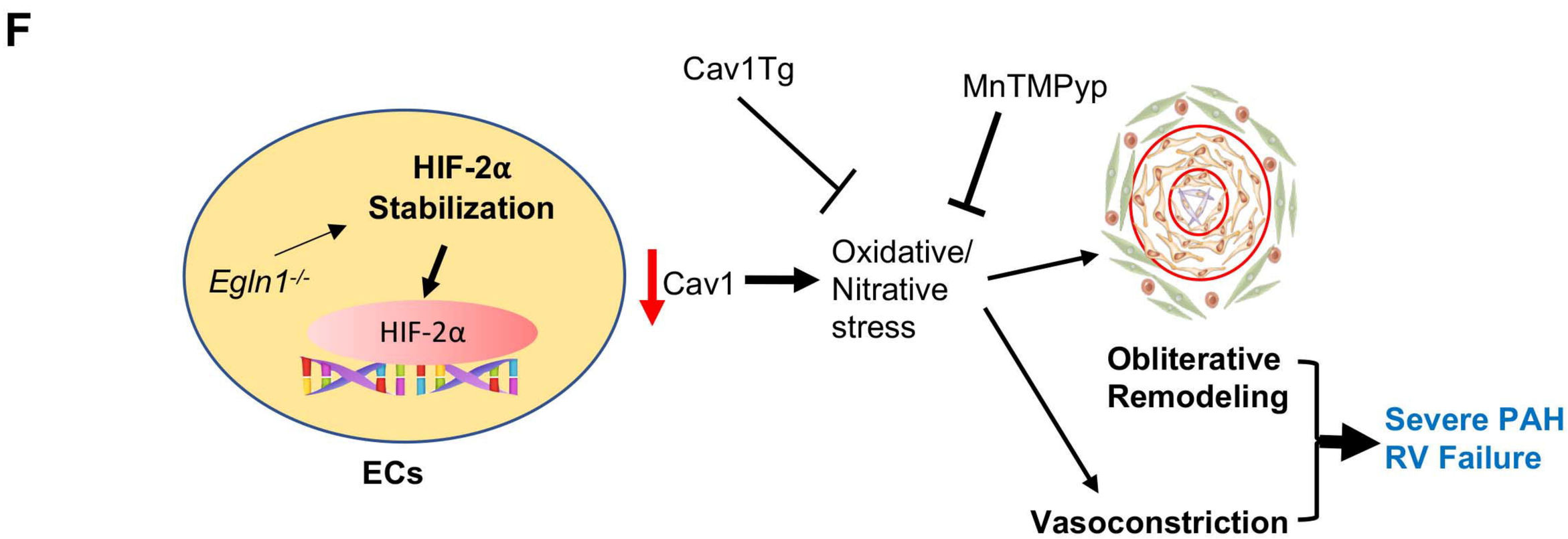
F
HIF-2α
Stabilization
Egln1-/-
HIF-2α
ECs
Cav1
Cav1Tg
MnTMPyp
Oxidative/
Nitrative
stress
Obliterative
Remodeling
Vasoconstriction
Severe PAH
RV Failure